

VYSOKÉ UČENÍ TECHNICKÉ V BRNĚ
BRNO UNIVERSITY OF TECHNOLOGY



FAKULTA STROJNÍHO INŽENÝRSTVÍ
ENERGETICKÝ ÚSTAV

FACULTY OF MECHANICAL ENGINEERING
ENERGY INSTITUTE

ANALÝZA PROUDĚNÍ Z VYÚSTKY OSOBNÍHO VOZU S VYUŽITÍM TERMOANEMOMETRICKÉ SONDY

ANALYSIS OF FLOW FROM THE CAR VENT USING THERMOANEMOMETRIC PROBE

DIPLOMOVÁ PRÁCE
MASTER'S THESIS

AUTOR PRÁCE
AUTHOR

BC. LIBOR ŠEDA

VEDOUcí PRÁCE
SUPERVISOR

ING. FRANTIŠEK LÍZAL, PH.D.

BRNO 2015

Vysoké učení technické v Brně, Fakulta strojního inženýrství

Energetický ústav

Akademický rok: 2014/15

ZADÁNÍ DIPLOMOVÉ PRÁCE

student(ka): Bc. Libor Šeda

který/která studuje v **magisterském studijním programu**

obor: **Technika prostředí (2301T024)**

Ředitel ústavu Vám v souladu se zákonem č.111/1998 o vysokých školách a se Studijním a zkušebním řádem VUT v Brně určuje následující téma diplomové práce:

Analýza proudění z vyústky osobního vozu s využitím termoanemometrické sondy

v anglickém jazyce:

Analysis of flow from the car vent using thermoanemometric probe

Stručná charakteristika problematiky úkolu:

Měření rychlostního pole proudu vzduchu z vyústky osobního vozu pomocí termoanemometrie. Sestavení měřicí aparatury a zkušebního zařízení, provedení experimentů, analýza výsledků a zhodnocení kvality vyústky.

Cíle diplomové práce:

Provedte měření rychlostního pole v proudu z vyústky osobního vozu termoanemometrickou sondou.

Provedení rešerše současného stavu poznání

Vyvinutí metodiky, která zajistí opakovatelnost měření (zejména metodika nastavování lamel, průtoků, ...)

Provedení měření rychlosti vhodnou sondou

Analýza výsledků

Vyhodnocení kvality vyústky

Seznam odborné literatury:

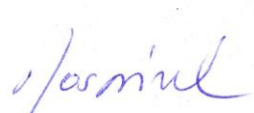
- [1] H. Awbi: Ventilation of buildings, SE, Spon press, London, 2003.
- [2] G. Gebauer a kol: Vzduchotechnika, ERA group, Brno, 2005.
- [3] J. Chyský, K. Hemzal a kol.: Větrání a klimatizace, BOLIT – B press, Brno, 1993.
- [4] H. H. Bruun: "Hot-wire anemometry, principles and data analysis". Oxford University Press 1994, ISBN-10: 0-19-856342-6.
- [5] Firemní literatura výrobce vozidla.

Vedoucí diplomové práce: Ing. František Lízal, Ph.D.

Termín odevzdání diplomové práce je stanoven časovým plánem akademického roku 2014/15.

V Brně, dne 9.9.2014





doc. Ing. Jiří Pospíšil, Ph.D.
Ředitel ústavu



doc. Ing. Jaroslav Katolický, Ph.D.
Děkan

ABSTRAKT

V diplomové práci jsou shrnuty základní poznatky o možnosti měření rychlosti proudění vzduchu a následně představena testovací trať pro automobilové vyústky, měřený objekt a uspořádání trati s různými komponenty. Metodou měření rychlostního pole je žárová anemometrie, a jsou proměřeny rychlostní profily v potrubí jako vstupy CFD simulace a 4 případy proudění. Jsou popsána kritéria hodnocení kvality vyústek a jejich vyhodnocení pro dané případy. Nadstavba práce je CFD simulace a porovnání výsledků mezi experimentem a simulací. V závěru jsou vyhodnoceny nejistoty měření a určení průtoku trati, řešené problémy a také návrhy pro další práci a vylepšení. Vizualizační a vyhodnocovací program vytvořený v prostředí MATLAB umožňuje jednoduché zobrazení dat získaných metodou CTA, které poslouží k dalšímu posuzování kvality ofukovačů.

ABSTRACT

In this master's thesis there are summarized fundamental findings about air flow velocity measurements and afterwards introduced the measuring track for automobile car vents, measured object and track arrangement and all used components. Velocity field measurement method is how wire anemometry, and apart from 4 main cases measurements of free air jet, there are velocity profiles in piping measured as an input for CFD simulation. Air vent evaluation criteria are described and their assessment is done for specified cases. Further, there is a CFD simulation presented with comparison to experimental data. Uncertainty of flow rate measured and flow rate setting is determined. Improvement points and encountered issues are presented. Visualization and evaluation program coded in MATLAB environment enables easy data display of CTA results and will serve further vent quality assessment.

KLÍČOVÁ SLOVA

Žárová anemometrie, měření metodou CTA, vyhodnocení kvality vyústky, volný proud vzduchu, úhel rozevření proudu.

KEYWORDS

Hot wire anemometry, CTA measurement, air vent quality assessment, free air jet, jet spread angle.

Bibliografická citace

ŠEDA, Libor. *Analýza proudění z vyústky osobního vozu s využitím termoanemometrické sondy: Diplomová práce*. Brno: Vysoké učení technické v Brně, Fakulta strojního inženýrství, 2008. 72 s., 5 příloh. Vedoucí práce Ing. František Lízal, Ph.D.

Prohlášení

Prohlašuji, že jsem diplomovou práci na téma Analýza proudění z vyústky osobního vozu s využitím termoanemometrické sondy vypracoval samostatně s použitím odborné literatury a pramenů, uvedených na seznamu, který tvoří přílohu této práce.

25. května 2015

podpis

.....

Bc. Libor Šeda

Poděkování

Here I would like to thank to supervisor of this thesis Ing. František Lízal, Ph.D. for his valuable comments. Further thanks goes to Ing. Ondřej Pech for his helpful attitude and to Ing. Lubomír Klimeš, PhD. and Ing. Jan Pokorný, PhD. for their help with MATLAB software and to Bc. Petr Caletka for his help with conducting experiments in laboratory.

Also I would like to thank to my family for their support during my studies at the university.

The author gratefully acknowledge the support from the Czech national project of the Josef Bozek Competence Centre for Automotive Industry TE01020020 and by the project LO1202 NETME CENTRE PLUS with the financial support from the Ministry of Education, Youth and Sports of the Czech Republic under the "National Sustainability Programme I"

Contents

Prefix	13
1 Theoretical part.....	14
1.1 Comfortable environment in transportation vehicles	14
1.1.1 Quality of the Indoor environment	15
1.1.2 Thermal comfort.....	15
1.2 Air flow	16
1.2.1 Air flow Types.....	16
1.2.2 Other air vent evaluation criteria	20
1.3 Air velocity and turbulence measurement	21
1.4 Hot Wire Anemometry	23
1.4.1 Principles of hot wire measurements – infinite length hot-wire sensors	23
1.4.2 Finite length hot-wire sensors	24
1.4.3 Modes of operation.....	26
2 Hot wire anemometry experiment	29
2.1 Measuring set	29
2.2 Eligible probe selection	32
2.3 Measurement and data evaluation workflow	33
2.4 Velocity flow measurement in channel	34
2.5 Velocity flow measurement in free space.....	36
2.5.1 Bend, flow rectifier and double flap.....	37
2.5.2 Coordinate system definition.....	38
2.5.3 Traverse grid description	39
2.5.4 Evaluated cases.....	40
2.5.5 General remarks.....	48
2.6 Repeatability of measurement	49
2.7 Spread Angles evaluation	49
2.7.1 Coordinate system and angles	49
2.7.2 Data processing	50
2.7.3 Software for border recognition outcome example	51
2.7.4 Angles evaluation	51
2.8 CTA measurement uncertainty	52
2.8.1 Hot wire anemometry measurement uncertainty	52
2.8.2 Flow rate measurement uncertainty.....	54

2.8.3	Flow rate setting uncertainty	56
2.8.4	Uncertainties summary	57
2.9	Issues encountered.....	57
2.9.1	Measurement in piping	57
2.9.2	Air filtration.....	57
2.9.3	1 wire probe – shear layer flow	58
2.9.4	Wrong data reduction	58
3	Computational fluid dynamics simulation.....	59
3.1	Fundamental equations.....	59
3.1.1	Continuity equation	59
3.1.2	Momentum equation.....	59
3.1.3	Energy equations	59
3.2	Physical modeling workflow	60
3.3	Pre-processing	60
3.4	Processing.....	64
3.5	Post-processing.....	64
	Conclusion.....	66
	Bibliography	68
	List of symbols	69
	List of annexes.....	72

Prefix

Ventilation and air-conditioning of vehicles is a topic that has been discussed since first cars and transportation vehicles were constructed and driven by humans. From the first heat and cold sources placed inside of the vehicles, designers were facing a problem – how to transport heat to places inside of a cabin where the heat is required?

Nowadays, nearly all cars sold are equipped with HVAC system – where heat is transported by air, that is flowing through air vents inside of the cabin. Even though such vent is a simple element, there can be great differences observed in quality, function and appearance while comparing vents from different car makers.

We can distinguish between various designs of vents, with different number of vertical and horizontal blades, dimensions and shapes. The question remains the same – which one is the best? In order to be able to answer this question, we must establish criteria, by which we compare various vents and then conduct measurement or simulations of different designs and compare them with each other.

Air jet as it is can be measured by various techniques, that are described in this thesis but it is more focused on constant temperature anemometry (CTA) method of air speed and turbulence level of air jet measurement. In the field of flow measurements, it is relatively cheap and exact invasive method that is widely used by both industrial and academic organizations.

Main objectives of this thesis are the measurement of air stream from a car vent that was 3D printed as part of a larger project, vent quality assessment and an evaluation and research about air flow measurement possibilities.

This is not the first work done on Faculty of Mechanical Engineering, previous method developed by F. Lizal, PhD and Ing. T. Lezovic is utilized and modified for present purpose.

1 Theoretical part

1.1 Comfortable environment in transportation vehicles

Comfort is a magical word. The thermal comfort in transportation vehicles has been a topic discussed since the first horse-drawn carriages were present on roads. At the beginning, the only possible way how to adjust the thermal comfort of passengers was their clothing that needed to be adapted to weather conditions.

When the carriages started to have roofs and windows, the nobility that was able to travel by such carriages could only adjust their clothing. The first attempts to modify the “inside” conditions were made shortly after – by placing heated bricks on colder days or ice cubes on warmer days inside of the vehicle. Hereafter the standard of thermal comfort control started to rise slowly. Ventilation was achieved through opening or tilting windows or the windscreen.

Eventually, fans to drive the air were introduced, and shortly after, heat exchangers using heat from exhaust system, or cold from cooling water followed. For some time, evaporative cooling was used in countries with very low humidity.

In 1939, Packard marketed the first mechanical automotive air conditioning system that was working with a closed cycle. A compressor, condenser, receiver drier and evaporator (all fitted inside the trunk of a vehicle) were part of the system. Even though this system had many disadvantages (the only system output controller was the blower switch, the compressor was driven directly and had no clutch, so to disengage the power, the belt had to be removed – during winter months)

After the World War II, Cadillac introduced a system with a switch accessible from the rear seats and first AC system for the mass usage in vehicles with an electronic clutch and controls on the dashboard was introduced to the market in 1954-55 by Nash-Kelvinator (Nash All-Weather Eye) (Daily 2006).



Figure 1.1 – Advertisement flyer for one of the first air conditioned cars (2015)

1.1.1 Quality of the Indoor environment

An average person spends approx. 70 – 80% of his/her life in the indoor environment (Janotkova 2014). Therefore, it can be concluded that the quality of such environment has an effect of quality of life itself, making it very important thing to consider.

Quality of an indoor environment is assessed considering the microclimatic aspects: (Janotkova 2014):

- 1) Air cleanliness
- 2) Air temperature
- 3) Temperature of adjacent surfaces and objects
- 4) Air flow velocity
- 5) Air humidity
- 6) Clothing of person inside
- 7) Light intensity
- 8) Noise, vibrations and ultrasound
- 9) Concentration of ions in the environment
- 10) Intensity of electrical and magnetic fields
- 11) Intensity of ionizing radiation
- 12) Spatial, dispositional and aesthetic disposition of environment
- 13) Person's physique
- 14) Person's activity
- 15) Person's ability to acclimatize
- 16) Climate, racial peculiarity and habits of person
- 17) Other factors – barometric pressure, psychical conditions etc.

The time spent in transport vehicles while commuting is significant and an effort to adjust the indoor environment of transportation vehicles makes only sense.

1.1.2 Thermal comfort

The condition of thermal equilibrium of human body states, that the energy produced in body reduced by energy that is transported in form of mechanical work done by the person is equal to energy diverted from the body by convection, conduction, evaporation and breathing. Thermal comfort is thus defined by the equation (1.1) (Janotkova 2014):

$$\dot{Q}_m(1 - \eta) = \dot{Q}_{conv} + \dot{Q}_{cond} + \dot{Q}_r + \dot{Q}_e + \dot{Q}_b \quad (1.1)$$

Where \dot{Q}_m is the metabolic heat flux of human body

η is the mechanical efficiency of human body

\dot{Q}_{conv} , \dot{Q}_{cond} , \dot{Q}_r , \dot{Q}_e , \dot{Q}_b are heat flux from human body by convection, conduction, radiation, evaporation and breathing respectively (Janotkova 2014) p10

This thesis deals only with aspects related to convective heat transfer, as the outcomes of conducted measurements are velocity fields and values of turbulence intensities in corresponding points of mesh (as demonstrated below).

1.2 Air flow

As stated above, the thermal comfort and comfort generally in indoor environment is influenced by air velocity and turbulence level, among others. To correctly assess the air-conditioning, one needs to calculate the volumetric flow rate (e.g. from requirements per person) but also assure, that the air velocity and turbulence levels at the point where assumed person would stay (in case of vehicles, sit) are acceptable.

1.2.1 Air flow Types

Air flow can be categorized using several criteria as:

- 1) Temperature of flow in comparison to ambient temperature
 - a. Isothermal flow - where flow temperature and ambient temperature are identical
 - b. Nonisothermal flow - Where flow temperature and ambient temperature are not identical
- 2) Spatial disposition
 - a. Free air jet – flow is far from any obstacle and walls
 - b. Bounded flow – flow can be e.g. “adjacent” to a nearby wall (“Coanda effect”)
- 3) Velocity profile
 - a. Laminar flow
 - b. Turbulent flow

1.2.1.1 Spatial disposition

Free air jet

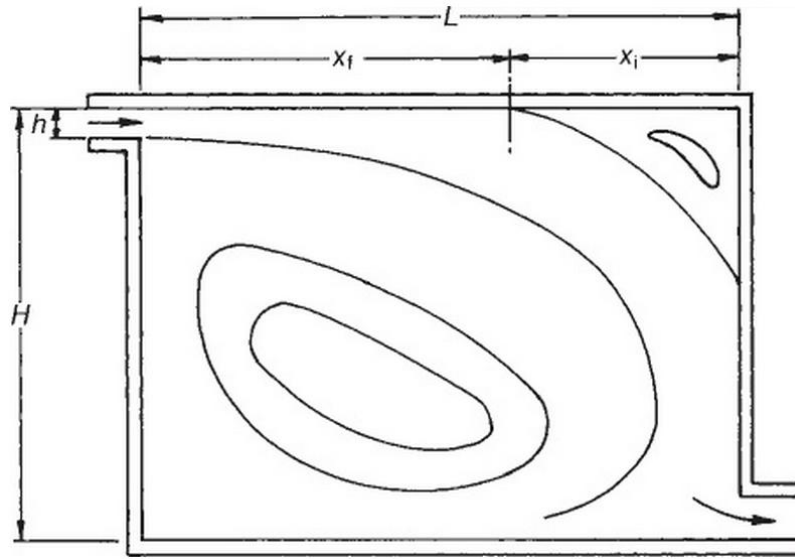
A flow is considered as free when the room dimensions are much greater than dimensions of the air vent. An example of isothermal free flow is shown below in Figure 1.3.

Half-bound flow

Half-bound flow is most common in rooms, where the vent is placed nearby a surface (e.g. wall, window). The flow reach is extended thanks to adjoining to the surface due to the Coanda effect.

Bounded flow

The bounded flow is most common in air-conditioned or ventilated rooms. It contains reverse flow, which is a result of interaction of the air in the room and in the flow (Janotkova 2014).



Where
 H is the room height
 L is the room length
 h is the AC opening diameter
 x_f, x_i are dimensions locating the eddy

Figure 1.2 Bounded air flow in air-conditioned room

1.2.1.2 Free, isothermal flow

Free isothermal flow is the basic case. Air flow with temperature T_f flowing to a large room with ambient air temperature T_a while $T_f = T_a$. The air is spreading from the air vent in a straight line, with lowering its velocity and deducting the surrounding air. The borders of air flow are limited by two conical areas, as shown in Figure 1.3:

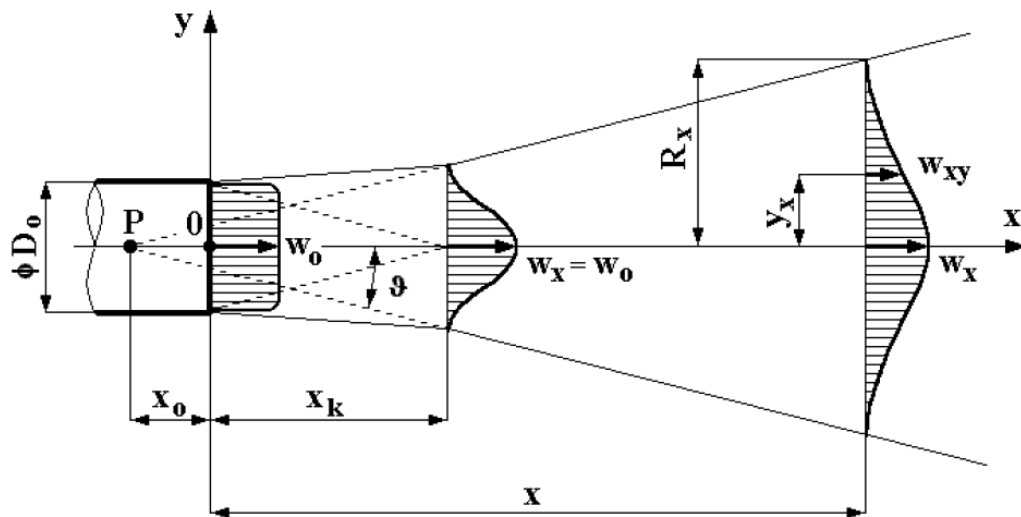


Figure 1.3 (Janotkova 2014)

The angle ν is usually considered as $2 \cdot \nu \approx 25^\circ$ (Janotkova 2014). No matter if shape of vent is circular, square or rectangular, the shape of air flow is always circular shape (as will be proved)(Janotkova 2014).

The variable x_k describes the length of “potential core” of flow where the air velocity remains constant, the rest of the flow is called “characteristic decay region”, according to importance in air-

conditioning domain. For analytical calculations of air flow reach and velocity in flow centerline and outside of it, half-empirical equations were introduced:

Length of outer region x_k

$$x_k \approx 7 \cdot S_0^{0,5} \quad (1.2)$$

Where S_0 is the cross-section area of vent, which can be calculated as:

$$S_0 = \alpha \cdot \kappa \cdot S_n \quad (1.3)$$

Where α is the contraction coefficient (usually 0,9)

S_n is the nominal cross-section area of vent

κ is the ratio between free cross-section (cross-section area of gaps in the vent) and nominal cross-section area S_n

In the main region, the axial velocity w_x is gradually lowering and can be expressed by equation

$$\frac{w_x}{w_0} = K_S \cdot \frac{\sqrt[2]{S_0}}{x} \quad (1.4)$$

Where w_x is the axial velocity of air flow

w_0 is the initial velocity of air flow (at the vent outlet)

K_S is the constant of vent. Maximal value is $K_S = 7$ for uniform velocity resolution at vent outlet

x is the distance of the point from vent outlet (Janotkova 2014)

Constant of vent K_S can be computed form equation mentioned in (Nový 2006):

$$K_S = \sqrt{\frac{\kappa \beta_0}{\beta \pi}} \cdot \frac{1}{k \cdot t g \vartheta} \quad (1.5)$$

β_0 is the momentum correction factor for non-uniform velocity distribution (selected value of $\beta_0 = 1,2$)

β is the correction coefficient on momentum (for circular jet $\beta = 2,02$)

k is the coefficient of velocity field (for circular jet $k = 0,258$)

ϑ is the spread angle of air jet

The transversal velocity profile can be expressed by Schlichting equation

$$\frac{w_{x,y}}{w_x} = \left[1 - \left(\frac{2 \cdot y_x}{D_x} \right)^{1,5} \right]^2 \quad (1.6)$$

(Janotkova
2014)

Where $w_{x,y}$ is the velocity at distance x in axial and y in transverse position

y_x is the transverse position of the specific point

D_x is the diameter of air flow at the specific point

1.2.1.3 Free, nonisothermal flow

The free nonisothermal flow is characterized by different temperature of the ambient air and the flow itself. This difference causes “bending”, deformation of air flow. It can be characterized as a resultant of inertial and gravitational forces – their ratio is expressed as Archimedes number Ar_0 . Gravitational forces result in vertical deformation of flow.

$$Ar_0 = \frac{g \cdot D_r}{w_0^2} \cdot \frac{T_1 - T_2}{T_2} \quad (1.7)$$

(Gebauer
2005)

where g is the gravitational constant

T_1 and T_2 are temperatures of air flow and ambient respectively

D_r is a equivalent diameter. For rectangular orifice we can write

$$D_r = \frac{2 \cdot a \cdot b}{a + b} \quad (1.8)$$

where a, b are orifice dimensions

While $Ar_0 < 0,001$, air flow is considered slightly nonisothermal, in cases when $Ar_0 > 0,01$, we deal with the flow as nonisothermal. Schematic diagram of Archimedes number is shown in Figure 1.4.

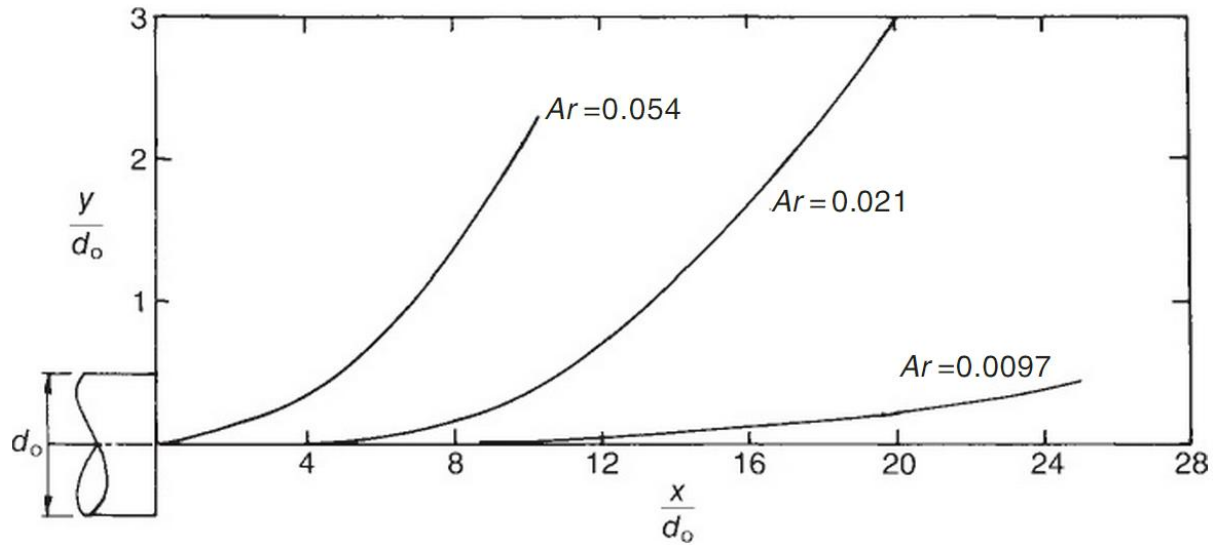


Figure 1.4 Archimedes number effect on flow curvature (Awbi 2003)

1.2.2 Other air vent evaluation criteria

As defined in (Ležovič 2011b), the main criteria for air vent evaluation are:

- Limited vertical direction
- Yaw and pitch angles
- Flow border determination

As the first mentioned criterion is applicable only with vents where the blades are in other than default (straight) position, it is not taken into account further. Both yaw and pitch angles are connected to determination of the flow border, as the borders are assessed based on them.

The flow border is determined as a place where the velocity has a 10% value of centerline velocity in corresponding point of flow (Awbi 2003):

$$w_c = 0,1 \cdot w_a \quad (1.9)$$

Where w_c is the velocity in non-axial point,

w_a is the velocity in centerline

1.3 Air velocity and turbulence measurement

Flow velocity measurements are performed using different principles and approaches as shown in this chapter by devices collectively called as anemometers.

Mechanical anemometers

Mechanical anemometer usually contain blades and are used for velocities $w_0 = 0,1 - 50 \text{ m/s}$ and $\varnothing = 10 - 200 \text{ mm}$ depending on type of anemometer. The measured velocity is proportional to rev velocity according to equation. (Pavelek 2015)

$$w_0 = a + b \cdot n \quad (1.10)$$

Where a , b are calibration constants and n is rev velocity.

They are quite easy to operate and relatively cheap (compared to e.g. HWA or ultrasound systems).

Ultrasound anemometers

Ultrasound anemometers are based on measuring ultrasound velocity in a liquid flow. Sensors are normally used for liquids, but are also available for air velocity measurements.

They are applicable to velocities $w_0 = 0,01 - 100 \text{ m/s}$ and in bigger scales are also suitable to turbulence intensity measurements. (Pavelek 2015)

Dynamic velocity probes

Most common are Pitot and Prandtl tubes (although in some applications cylindrical or spherical probes are used) according to equation:

$$w_0 = k \cdot \sqrt{\frac{2p_d}{\rho}} \quad (1.11)$$

Where k is a calibration constant and p_d is the dynamic pressure, that is the difference between total pressure p_t and static pressure p_s .

$$p_d = p_t - p_s \quad (1.12)$$

The equation (1.11) is valid from approximately 1 m/s to $1/3$ of velocity of sound in the medium under specified conditions. (Pavelek 2015)

Laser anemometers

Laser Doppler Anemometry (LDA) systems are based on principles of light interference and light decomposition on small particles. This method is suitable for velocity measurements of $w_0 = 0,001 - 300 \text{ m/s}$ and velocity fluctuations of $\pm 70 \%$ with frequencies $> 100 \text{ kHz}$, which makes it a system with widest operation range of all of the above mentioned techniques. (Pavelek 2015)

An example how such system looks like, see Figure 1.5:

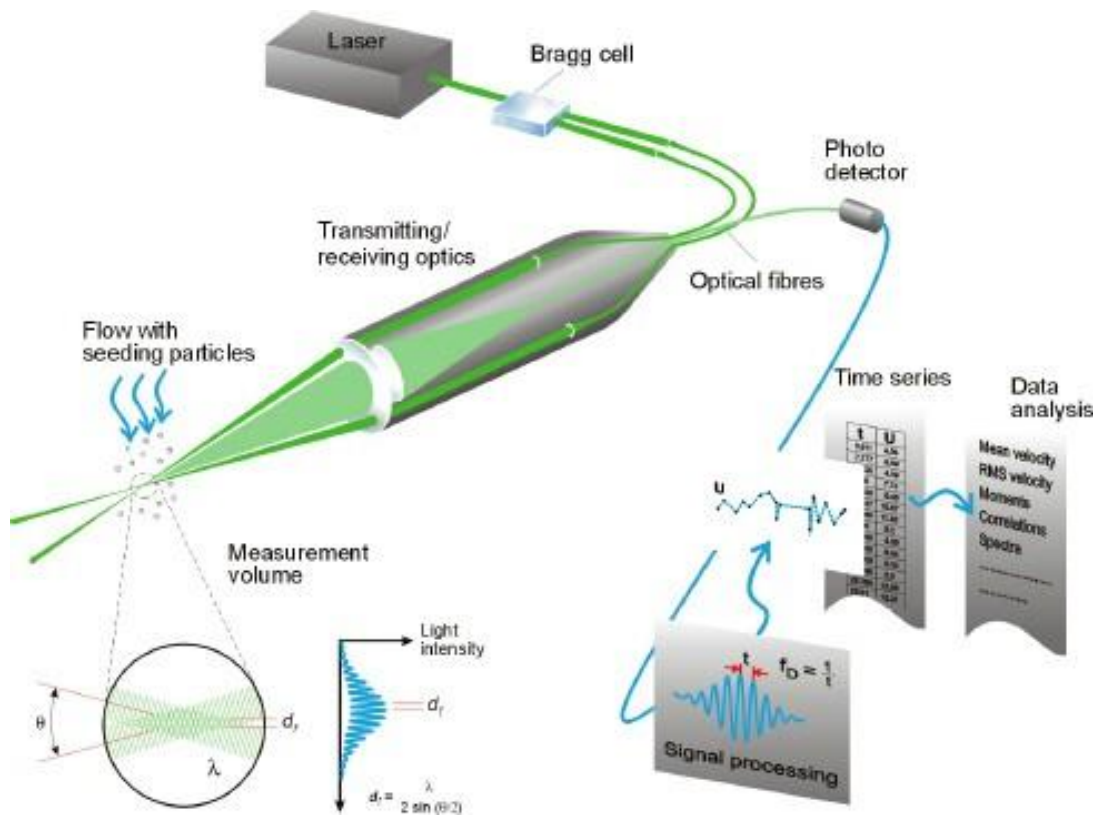


Figure 1.5 LDA system (Dantec and Dynamic 2015)

Turbulence measurement

Turbulence measurement means the measurement of the turbulence intensity, which is defined as:

$$Tu = \frac{1}{\bar{w}} \sqrt{\frac{\sum_i (w_i - \bar{w})^2}{n - 1}} \quad (1.13)$$

Where \bar{w} is the average velocity

w_i are the measured velocities

n is the number of measurements

Tu turbulence intensity (computed as an relative error of measurement -- the square root is the standard deviation) (Pavelek 2015)

The main concern about measuring turbulence is, that anemometers with small time constants, e.g. those, that respond to velocity changes better need to be used. Those are mainly hot wire anemometry systems, ultrasound anemometers, laser anemometers and Time-resolved PIV systems. (Pavelek 2015)

Thermoanemometres

The measurement with thermoanemometers is described in detail in next chapter.

1.4 Hot Wire Anemometry

There are many ways how to describe velocity fields, as shown before. Experiment, that was conducted as part of this thesis is dealing with hot wire anemometry systems. The method itself is not new, it has been used for already 100 years (Comte-Bellot 1976) but new devices for more precise measurement and calibration of probes are still under development.

1.4.1 Principles of hot wire measurements – infinite length hot-wire sensors

Hot wire anemometry is based on convective heat transfer from a sensing element, with most common sensor configurations being cylindrical hot wire sensors and sensors contacting hot-film deposited on cylindrical fibers.

Heat transfer from a heated wire that is placed in a fluid flow depends on:

- Properties of the ambient fluid (density ρ , viscosity μ , thermal conductivity k and specific heat of the fluid c_p)
- Parameters of the flow (velocity vector v , fluid temperature T , pressure p , etc.).

To be able to compute heat transfer from a wire, relationships were expressed in terms of the nondimensional numbers of Nusselt (Nu), Reynolds (Re), Prandtl (Pr), Grashof (Gr), Mach (M), where:

$$Nu = \frac{h \cdot d}{k} \quad (1.14)$$

$$Re = \frac{\rho \cdot U \cdot d}{\mu} \quad (1.15)$$

$$Pr = \frac{c_p \cdot \mu}{k} \quad (1.16)$$

$$Gr = \frac{g \cdot \rho^2 \cdot d^3 \cdot \beta \cdot (T_w - T_a)}{\mu^2} \quad (1.17)$$

$$M = \frac{U}{a} \quad (1.18)$$

Where h is the convective heat-transfer coefficient, k is the thermal conductivity of the fluid, μ is the dynamic viscosity of the fluid, c_p is the specific heat of the fluid at a constant pressure, ρ is the density of the fluid, g is the gravitational acceleration, β is the volume coefficient of expansion, T_w is the temperature of the heated wire, T_a is the temperature of ambient fluid, a is the velocity of sound, U is the flow velocity, d is the diameter of cylindrical element

During the first attempts to measure with hot/wire anemometers, the experimentators based their thinking on following dependence;

$$E = f(U) \quad (1.19)$$

Where E is the output from anemometer and U is the velocity component in the mean/flow direction.

The early and pioneering experimental and theoretical work done by King in 1914 (Dantec 2013) show, that the convective heat transfer can be expressed in the form

$$Nu = A + B \cdot Re^{1/2} \quad (1.20)$$

Where A, B are empirical calibration constants for a specific fluid and thus proving a relationship between heat transfer rate from the wire and flow parameters

1.4.2 Finite length hot-wire sensors

The heat transfer from infinite length hot-wire sensors serves as a deviation to governing equations of finite length hot-wire sensors.

In practise, the sensing element, in form of wire, is connected to two prongs. It can either be extended to the prongs, or the active part of the wire may be removed from the prongs.

In comparison with the wire element, the prongs are massive, and the prong temperature, T_p will during the measurement remain at a temperature close to the temperature of the ambient fluid, T_a .

As the wire is operated at elevated temperature, the temperature distribution along the wire is not uniform. It can be determined from the heat-rate balance equation for an elementary wire element, dx from equations:

$$d\dot{Q}_e = d\dot{Q}_{fc} + d\dot{Q}_c + d\dot{Q}_r + d\dot{Q}_s \quad (1.21)$$

(Brunn 1995)

where $d\dot{Q}_e$ is the electrical heat-generation rate,

$d\dot{Q}_{fc}$ is the forced-convective heat-transfer rate,

$d\dot{Q}_c$ is the conductive heat-transfer rate,

$d\dot{Q}_r$ is the radiation heat-transfer rate,

$d\dot{Q}_s$ is the heat storage rate.

From which individual terms can be expressed as:

$$d\dot{Q}_e = \frac{I^2 \cdot \chi_w}{A_w} \cdot dx \quad (1.22)$$

Where I is the electrical current through wire

χ_w is the electrical resistivity of the wire material at a local wire temperature T_w and

A_w is the cross-sectional area of the wire.

The forced-convection heat transfer rate $d\dot{Q}_{fc}$ to the fluid can be expressed in terms of the heat-transfer coefficient h , as

$$d\dot{Q}_{fc} = \pi \cdot d \cdot h \cdot (T_w - T_a) \cdot dx \quad (1.23)$$

Total conduction heat-transfer rate out of the element dx is then

$$dd\dot{Q}_c = -k_w \cdot A_w \cdot \frac{\delta^2 T_w}{\delta x^2} \cdot dx \quad (1.24)$$

where k_w is the thermal conductivity of the wire material at the temperature T_w . The radiation heat-transfer rate is:

$$d\dot{Q}_r = \pi \cdot d \cdot \sigma \cdot \varepsilon \cdot (T_w^4 - T_s^4) \cdot dx \quad (1.25)$$

where σ is Stefan-Boltzmann constant, ε is the emissivity of the sensor, and T_s is the temperature of the surroundings. The heat-storage rate is

$$d\dot{Q}_s = \rho_w \cdot c_w \cdot A_w \cdot \frac{\delta T_w}{\delta t} \cdot dx \quad (1.26)$$

Where ρ_w is the density of wire material and c_w is the specific heat of wire material per unit mass.

From these equations, we can derive temperature distribution along the wire that can be seen in Figure 1.6.

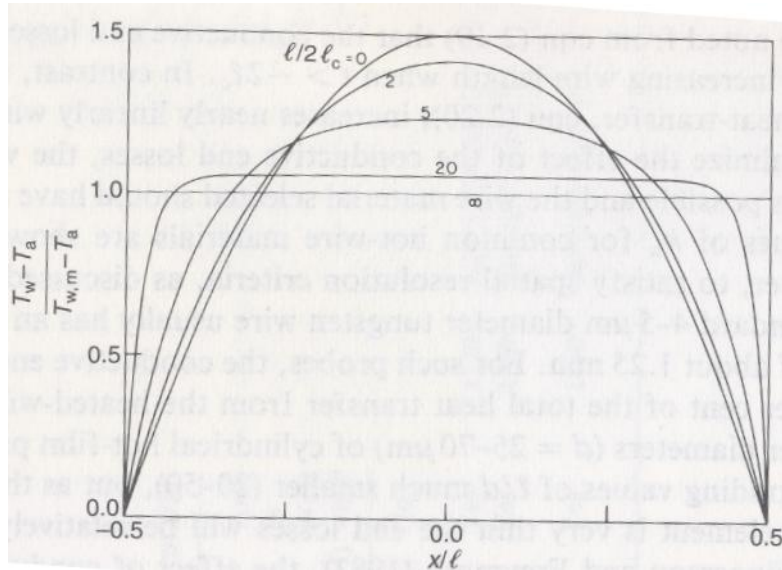


Figure 1.6 Temperature distribution along the wire for various values of l/l_c (cold length) (Brunn 1995)

1.4.3 Modes of operation

Generally, with use of hot wire anemometers, two different approaches were developed, having varied advantages. A constant temperature and constant current mode, both having different electrical scheme, constant current mode is used mainly for temperature measurements, and it will not be covered in this work.

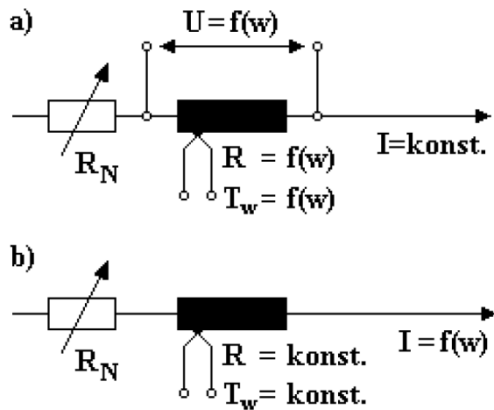


Figure 1.7 shows difference in a) CCA circuit and b) CTA circuit

Figure 1.7 CCA and CTA difference (Pavelek 2015)

Constant temperature mode

In the CT mode the wire hot resistance, R_w (and thereby its temperature), remains constant e.g. independent of the flow conditions. As the flow conditions vary, the feedback differential amplifier, that is incorporated to the hot wire anemometer circuit allows us to obtain rapid variation in the heating current to compensate for instantaneous changes in the flow velocity.

The hot wire probe is placed in a Wheatstone bridge. Wire resistance is linked to the error voltages $e_2 - e_1$ that we are measuring as the input to the operational amplifier.

This amplifier has an output current i that is inversely proportional to the change of resistance of the hot wire sensor. This current is then feed to the top of the bridge, restoring the sensor's resistance to its original value (Figure 1.8).

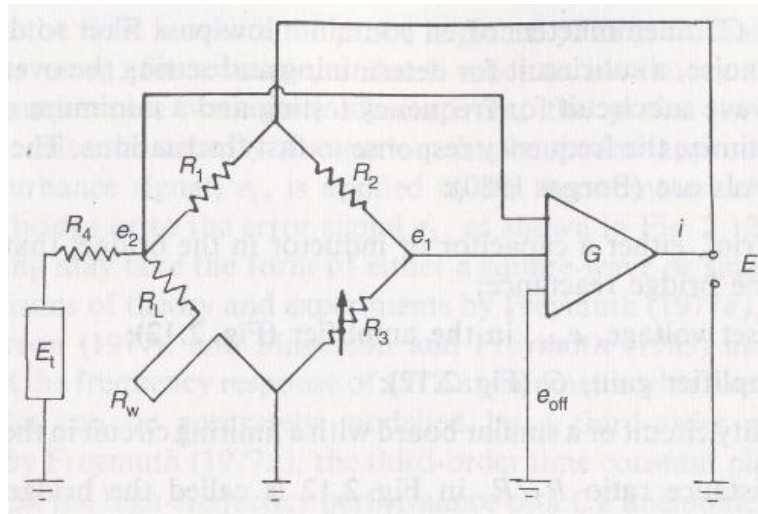


Figure 1.8 A CT anemometer containing Wheatstone bridge, a feedback amplifier and an electronic-testing subcircuit (Brunn 1995)

Sensor types

There are two main types of probes that are widely used,

- Hot-film probes,
- Hot wire probes.

Hot-film probes

Hot-film sensors are thin (approx. $0,1 \mu\text{m}$) platinum or nickel films that are deposited on thermally insulating substrates (e.g. quartz). The most used shapes of substrates are cylinders, wedges and cones.

Fiber-film and film-sensors are normally $70 \mu\text{m}$ in diameter and with 1.2 mm active length, covered by nickel thin-film which is protected by quartz coating. Fiber sensors are mounted on prongs in the same way as wires.

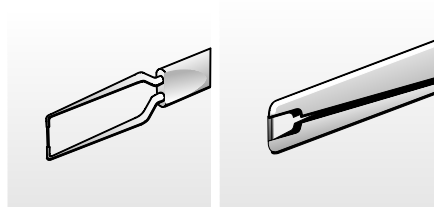


Figure 1.9 (Jørgensen 2002)

Surface measurements with flush mounted probes or sensors mounted on thin plastic foils glued to the wall can be also performed. The film is then usually coated with a $1-2 \mu\text{m}$ thick deposited layer of

quartz or another insulating material. This coating protects the film material from abrasive particles and provides electrical insulation for hot-film probes used in liquids. (Brunn 1995)

Hot-film probes are used in the case when mean velocity measurements and long-term calibration stability are the primary concerns of the experimenter. The same applies to measurements in liquids, when hot-film probes are more suitable due to their sturdier construction.

Hot-film probes with sensors coated with quartz or aluminium oxide can be even used in contaminated gas flows, since the coating prevents the film from being eroded. The usage of hot-wire probes in such environment is questionable.

Hot-wire probes

In comparison with hot-film probes, hot-wire probes are mainly used when accurate turbulence results are required in gas flows. (Brunn 1995)

As the changes in turbulence levels in gas flow are very fast, it is therefore important that the sensing element and its associated electronic circuit can provide a virtually instantaneous response to the fastest occurring flow changes that nowadays systems do (possible measurements up to 60kHz) .

A single-sensor hot-wire probe (for the measurement of 1 component of velocity vector) consists of a wire of fine diameter and short length attached to two prongs that are usually made of stainless steel or nickel. For most practical hot-wire anemometry applications, the materials used are tungsten, platinum-iridium alloy (80-20 per cent). For very fine wires, platinum and its alloys are usually selected, since it is available with diameter as small as 0,25 μm . A standard probe is around 1,25 mm long and has 4-5 μm in diameter. (Brunn 1995)

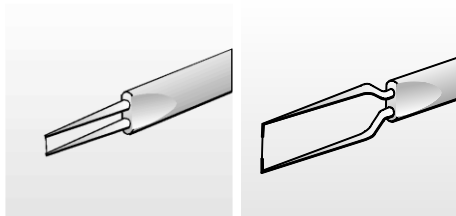


Figure 1.10 (Jørgensen 2002)

On Figure 1.10, we can see two most used configurations - miniature wires and gold-plated wires respectively. Both have approximately the same active wire length but the gold-plated wires are copper- and gold-plated at the ends to total length of 3 mm in order to minimize prong interference.

Sensor configurations

Probes are available in one- to three-dimensional versions as single- to triple-sensor probes referring to the number of sensors. This is due to the fact that sensors respond not only to magnitude of the velocity vector but also to its direction. Information about both can be obtained only when two or more sensors are placed to the flow vector under different angles (Jørgensen 2002).

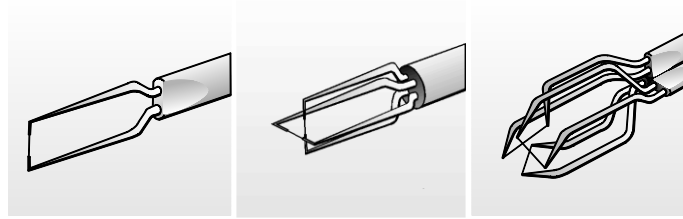


Figure 1.11 (Jørgensen 2002)

Measurement

As stated earlier, voltage $e_2 - e_1$ is measured and it is transformed to velocity by means of calibration constants afterwards. The calibration of a probe is a regular process and it should be done before every measurement

2 Hot wire anemometry experiment

Measurements done within this thesis follow previous measurements and experiments done by Ing. Frantisek Lizal, PhD. and Ing. Tomas Lezovic by Constant Temperature Anemometry.

2.1 Measuring set

A measuring set is located in the laboratory of ventilating systems of Faculty of Mechanical Engineering, room C3/213c. The set consists of the two main parts – the air flow part (where the vent is located) and the measuring part. The air flow part is described by Bc. Petr Caletka (Caletka 2014) and in Figure 2.1 its configuration is shown.

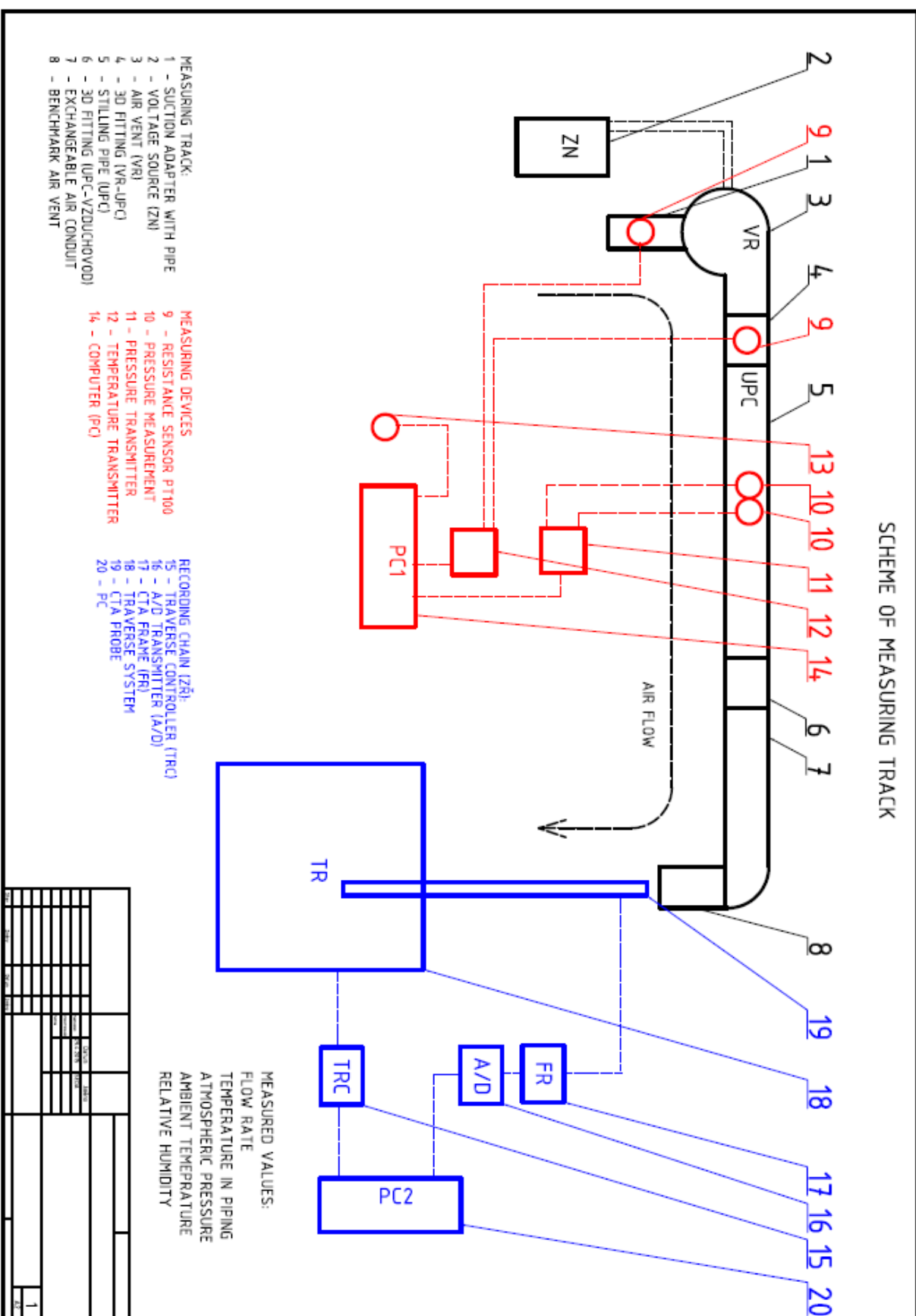


Figure 2.1 Measuring track, remade from (Caletka 2014)

It consists of the air ventilator, supplied by automotive manufacturer ŠKODA AUTO a.s., the piping, the differential pressure flow meter and the vent itself.

As described in (Caletko 2014), there are 2 air flow rates in point of interest.

- $33,5 \text{ m}^3/\text{h}$ - the most used flow rate during ventilation operation and the second,
- $80,6 \text{ m}^3/\text{h}$ - the maximal air flow rate through air vent.

The measurement of flow rate is done according to EN ISO 5167, uncertainties of this measurement will be calculated hereafter.

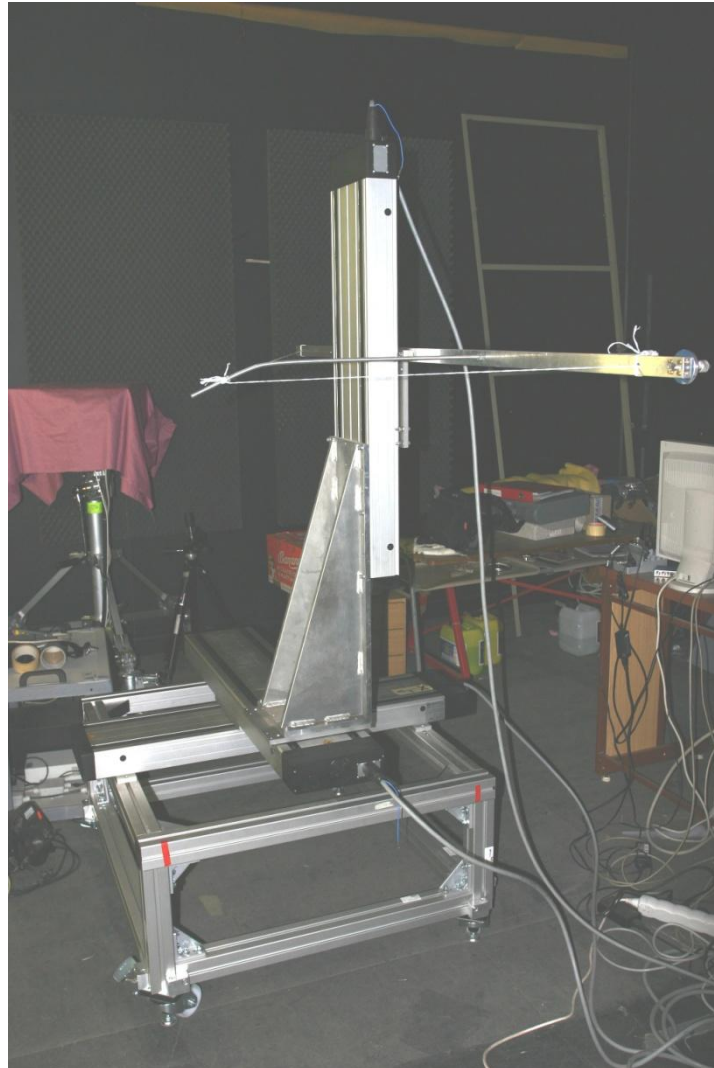


Figure 2.2 ISEL traverse system

Limits and reference	X	-430 mm	265 mm
	Y	0 mm	710 mm
	Z	-210 mm	400 mm
Velocity and calibration	X	5 mm/s	80 pulses/min
	Y	5 mm/s	80 pulses/min
	Z	5 mm/s	160 pulses/min

Table 2.1 Traverse system settings

Originally, the traverse system was standing on 2 palettes and the manipulation with it was uneasy, as it weighted around 120 kg in a whole. A new design was made by Ing. Pech and was composed of Alutec construction material and assembled by the author and Ing. Pech.

The adjustment had an impact on traverse system stability, which was improved. When the traverse system stops traversing, the probe starts to vibrate. This means that before measurement of each point, there needs to be around 5 seconds steadying interval needs to be there before the probe starts to measure. However, with this improved construction the steadying interval was shortened to 2 seconds, thus reducing overall measurement time by approximately 30% and enabling measuring a finer mesh in identical time interval.

2.2 Eligible probe selection

After debate with supervisor of this thesis, conclusion was made to use probe with only one wire (1D probe) from experience with measurement on The Department of Thermodynamics and Environmental Engineering. Advantages of measurement with 1D probe is that it is faster, not complicated and for 1D flow sufficient. Also, as the probe is smaller then 2 and 3 wire sensors, the resolution is finer.

Probe selected for measurement was simple type “55P01” – a gold-plated wire probe. It has diameter $5\text{ }\mu\text{m}$ and a 3 mm long platinum-plated tungsten wire sensor. The wire ends are copper- and gold-plated to a thickness of $15\text{ to }20\text{ }\mu\text{m}$, leaving an active sensor, $1,25\text{ mm}$, on the middle of the wire. They are designed for measurements in high-turbulence flows of one-dimension (Dantec_Dynamics 2013).

For measurement in piping, probe “55P04” was used. Both are shown in Figure 2.4 and Figure 2.5 (Dantec_Dynamics 2013).

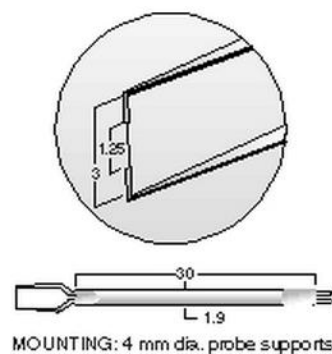


Figure 2.3 Probe mounting detail

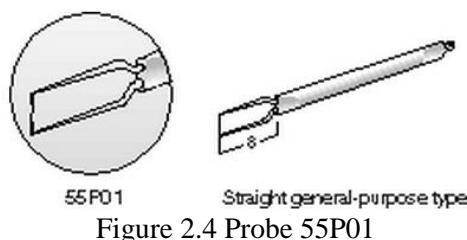


Figure 2.4 Probe 55P01

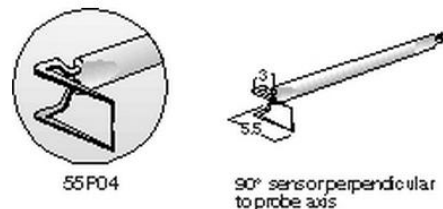


Figure 2.5 Probe 55P04

2.3 Measurement and data evaluation workflow

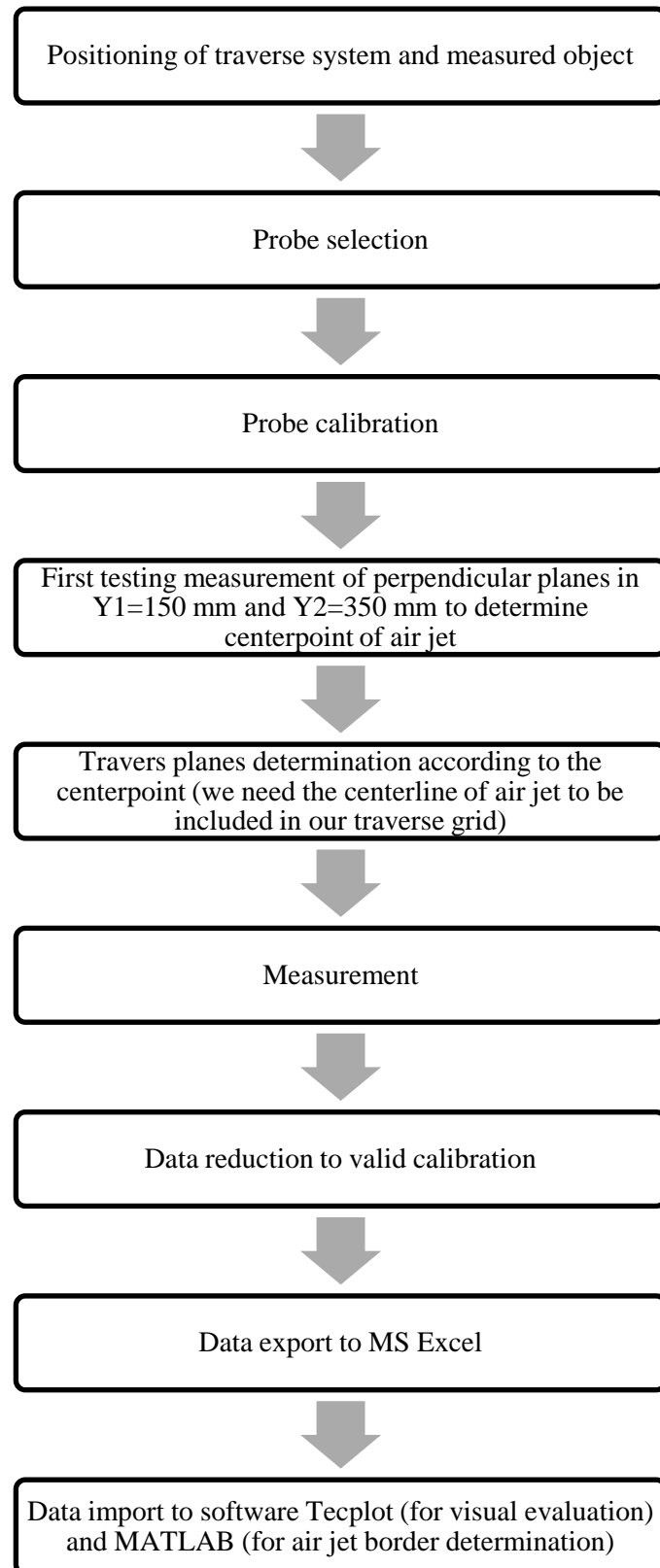


Table 2.2 Measurement and data evaluation workflow

2.4 Velocity flow measurement in channel

The first measurement conducted was the air velocity profile measurement that was requested as an input velocity boundary condition of CFD simulation carried out by Ing. Pavel Niedoba. The measurement was done on an adapted piping (Figure 2.6) with small holes drilled in it to enable insertion of measuring probe. Figure 2.7 then shows a schematic location of measuring holes on the test track.

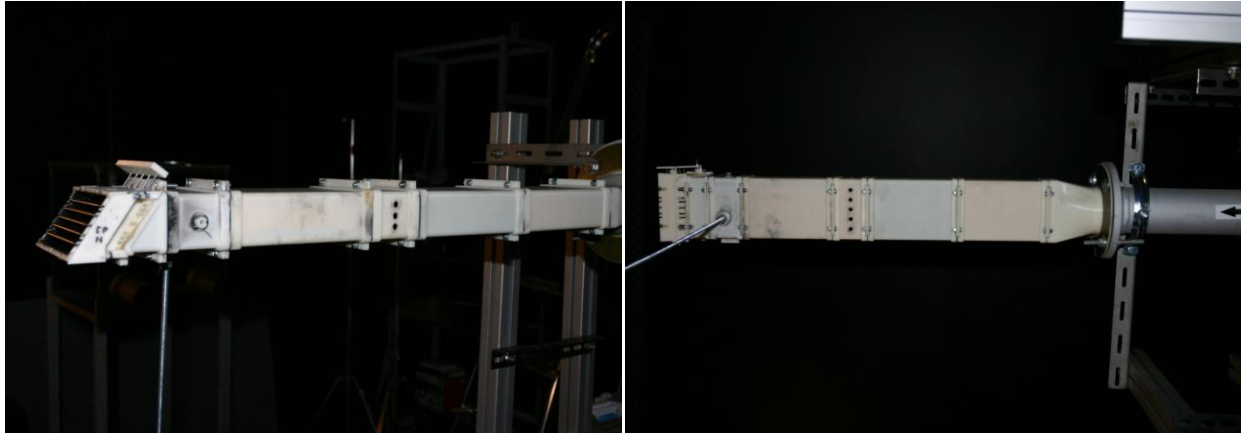


Figure 2.6 An adapted piping for air velocity measurement inside the channel

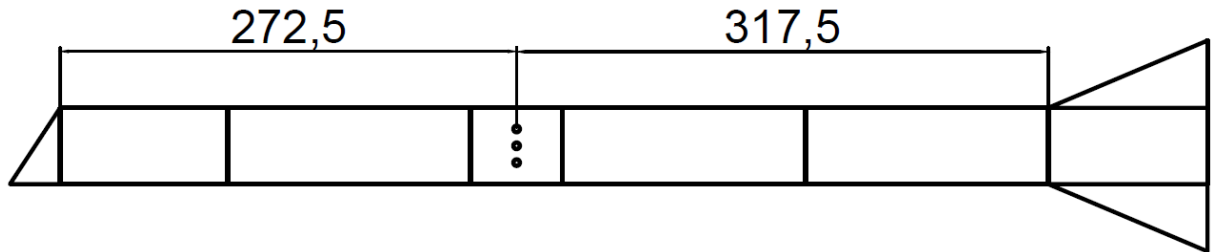


Figure 2.7 Measuring holes location on test track

The holes with diameter $d_h = 5,5 \text{ mm}$ were drilled additionally by Ing. Pech (the probe greatest size is 3 mm) making the insertion of a probe a rather hard task, as it needed to be done manually (one probe was unfortunately damaged while doing so). During the measurement, all the other holes were plugged with Lukopren apart from one being measured.

From Reynolds number (Equation (2.1)), we can make an assumption of flow profile:

$$Re = \frac{\rho \cdot U \cdot d}{\mu} \quad (2.1)$$

Air temperature $T = 22^\circ\text{C}$, air relative humidity $\varphi = 50 \%$, atmospheric pressure $p_b = 98,1 \text{ kPa}$:

Air density $\rho = 1,1518 \frac{\text{kg}}{\text{m}^3}$ (Pavelek 2010), dynamic viscosity $\mu = 18,24 \text{ N} \cdot \text{s} \cdot \text{m}^{-2}$ (Pavelek 2015)

and characteristic linear dimension $d = \frac{4 \cdot A}{P}$ where A is the cross-section area and P is the wetted perimether.

In our case, $d = 56,3 \text{ mm}$ and flow velocities $U_1 = 5,142 \text{ m/s}$ and $U_2 = 2,137 \text{ m/s}$ for flow rates $80,6 \text{ m}^3/\text{h}$ and $33,5 \text{ m}^3/\text{h}$ respectively, Reynolds numbers can be seen in Table 2.3.

$$A = 4354,3 \text{ mm}^2, P = 309,3 \text{ mm}, d = 56,3 \text{ mm}$$

$\rho \left[\frac{\text{kg}}{\text{m}^3} \right]$	$\mu [N \cdot s \cdot m^{-2}]$	$d[m]$	$U[m/s]$	$Re[-]$
1,1518	$18,24 \cdot 10e - 6$	0,0563	5,142	18281
			2,137	7597

Table 2.3 Reynolds number computation

Based on this computation, turbulent profile in selected region is expected as both values of Reynolds number are above 2000 which is considered to be a limit for laminar flow regime.

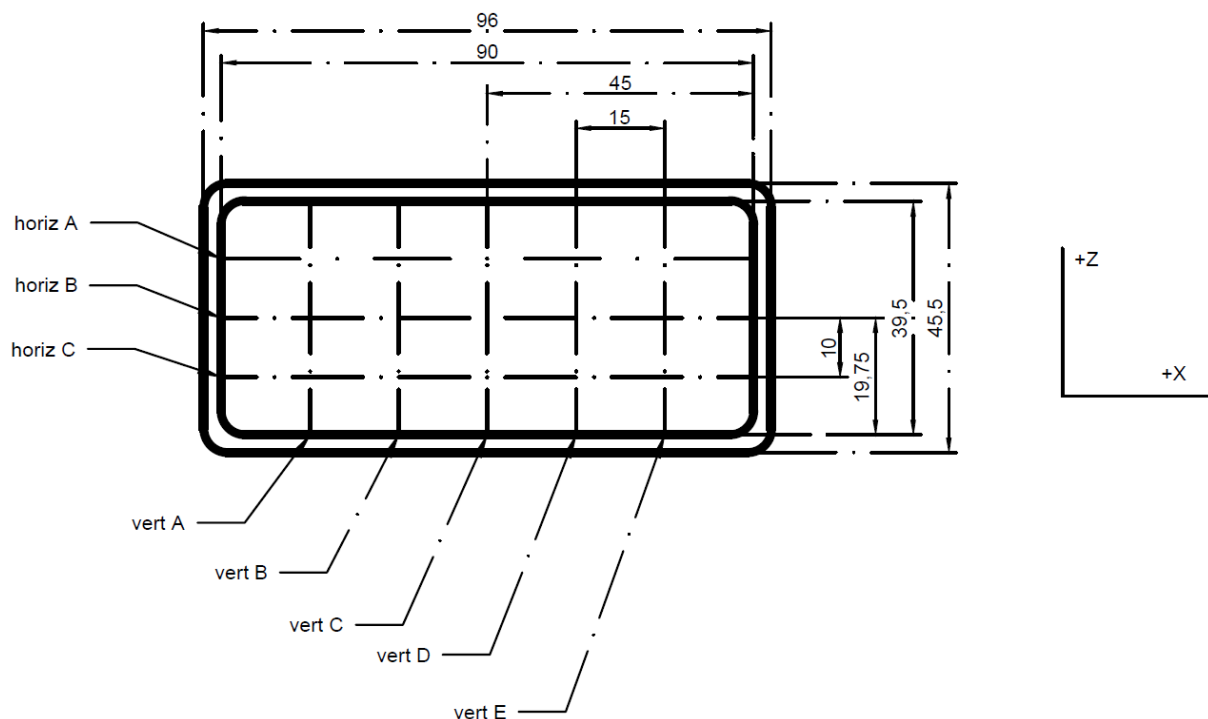


Figure 2.8 Velocity profile measurement lines

In Figure 2.8 we can see measurement lines location. All results were handed to Ing. Niedoba so this is only extract – „horiz B“ and „vert C“ lines from measurements of both flow rates.

Dimension step is in all cases 2 mm, and data processing was done in software MATLAB.

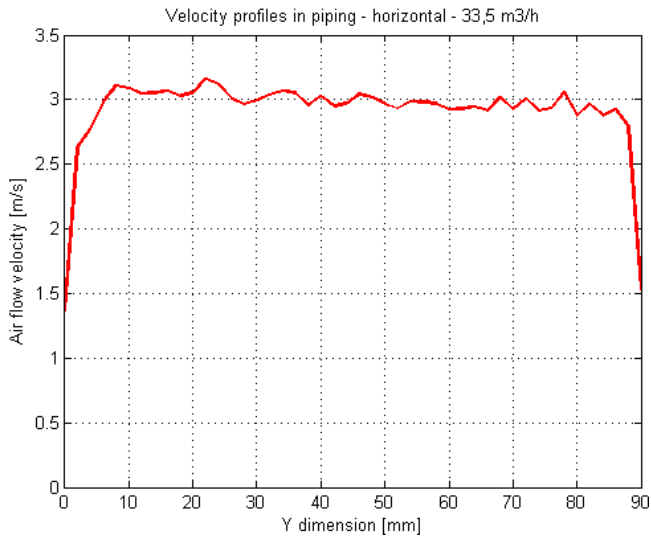


Figure 2.9 "Horiz B"

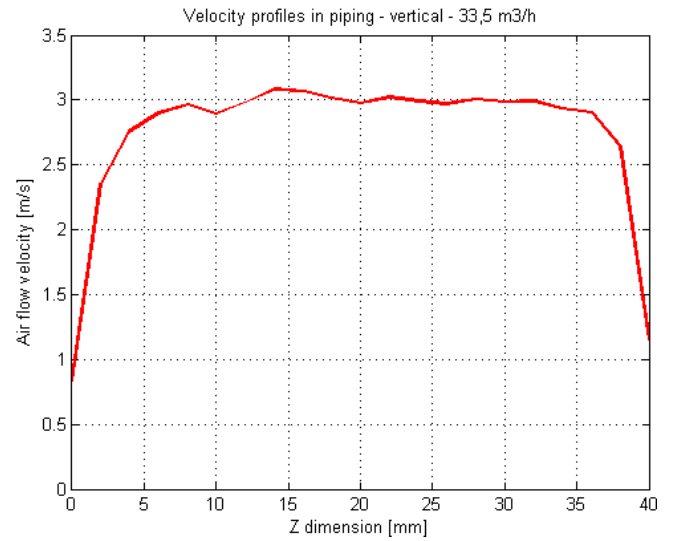


Figure 2.10 "Vert D"

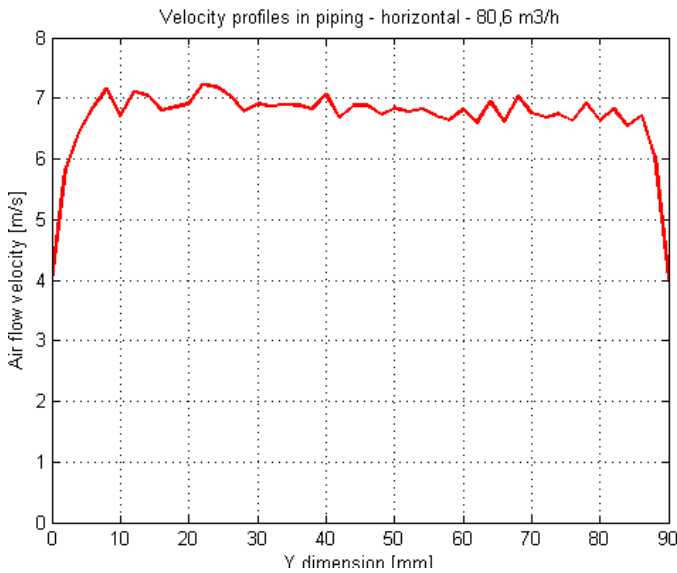


Figure 2.11 "Horiz B"

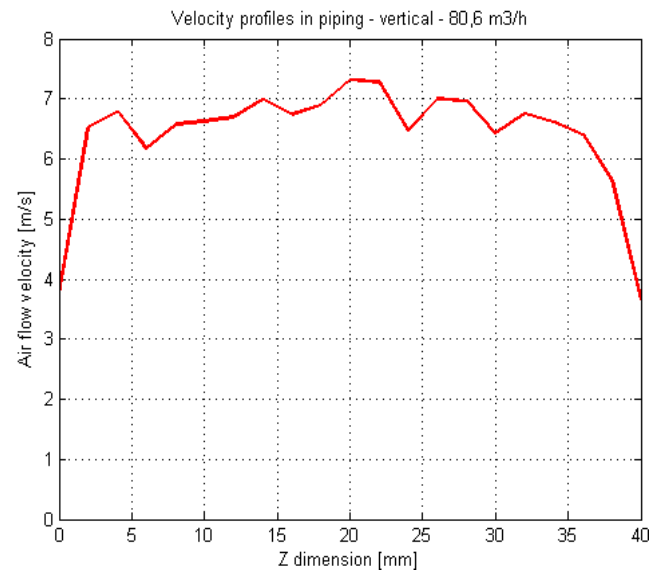


Figure 2.12 "Vert D"

In both cases, we can see that the speed profile matches the assumption of turbulent air flow. The measurement near the surface was done manually, since the vibrations of the traverse system could have harmed the measuring probe but according to theoretical assumption, the air velocity at the surface is zero.

2.5 Velocity flow measurement in free space

Firstly, let us compute Archimedes number, according to Equation (1.7)

$$Ar_0 = \frac{g \cdot D_r}{w_0^2} \cdot \frac{T_1 - T_2}{T_2} \quad (1.7)$$

In our case $g = 9,81 \text{ m/s}^2$, D_r is equal to $d = 56,3 \text{ mm}$ from previous chapter, w_0 is equal to $U_{1,2}$ ($U_1 = 5,142 \text{ m/s}$ and $U_2 = 2,137 \text{ m/s}$) from previous chapter and $T_{1,2}$ are the temperatures of the

air flow and the ambient respectively. In worst case identified during measurement (in winter months, when the heating was switched on in the laboratory), $T_1 = 20^\circ\text{C}$ and $T_2 = 13^\circ\text{C}$.

In this case, the flow velocity w_0 is connected to the velocity at vent outlet, and from later presented measurements, we set $w_{01} = 8\text{m/s}$ and $w_{02} = 3\text{m/s}$

$T_1[^\circ\text{C}]$	$T_2[^\circ\text{C}]$	$D_r[\text{m}]$	$w_0[\text{m/s}]$	$g[\text{m/s}^2]$	$Ar[-]$
20	14	0,0563	8	9,81	0,0037
			3		0,0263

According to the criteria stated in chapter 1.2.1.3, the flow can be considered moderately nonisothermal in first case and nonisothermal in the second case.

Secondly, equations mentioned in chapter 1.2.1.2 are used to calculate the length of outer region.

$S_n = 4844,6\text{ mm}^2$, $\alpha = 0,9$, $\kappa = 0,7028$ and thus

$$S_0 = 3064,31\text{ mm}^2$$

and the length of outer region x_k

$$x_k \approx \mathbf{387,5\text{ mm}}$$

2.5.1 Bend, flow rectifier and double flap

In this part, air flow rectifier, bend and double flap are presented. Detailed technical information can be found in Annex, where 3D models are attached.

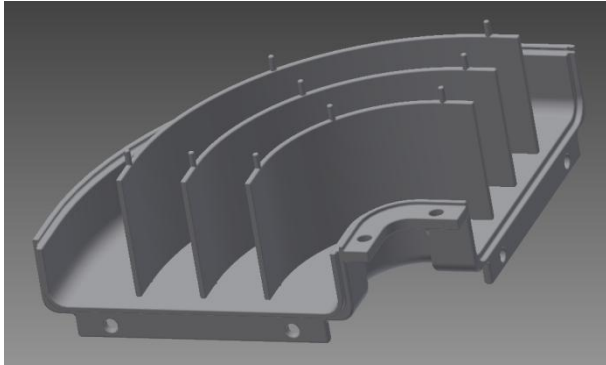


Figure 2.13 Air flow rectifier - detail

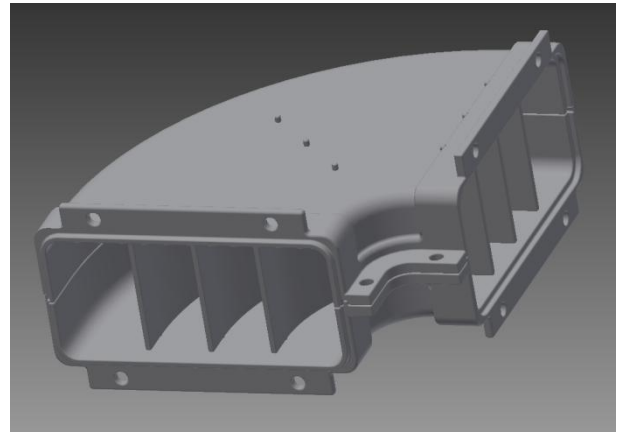


Figure 2.14 Air flow rectifier - with bend

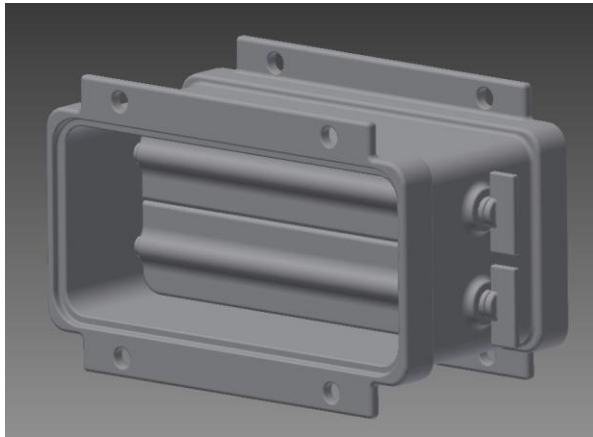


Figure 2.15 Double flap - closed position

Figure 2.13, Figure 2.14 and Figure 2.15 illustrate how bend, air flow rectifier and double flap look like.

Inventor models can be found in enclosure to this thesis, they were made as an part of work done by “Centrum komepetence automobilového průmyslu” by Bc. Michal Závodník.

2.5.2 Coordinate system definition

The coordinate system used in this thesis is equivalent to the coordinate system of traverse system. It can be seen in Figure 2.16 as well as the zero point.

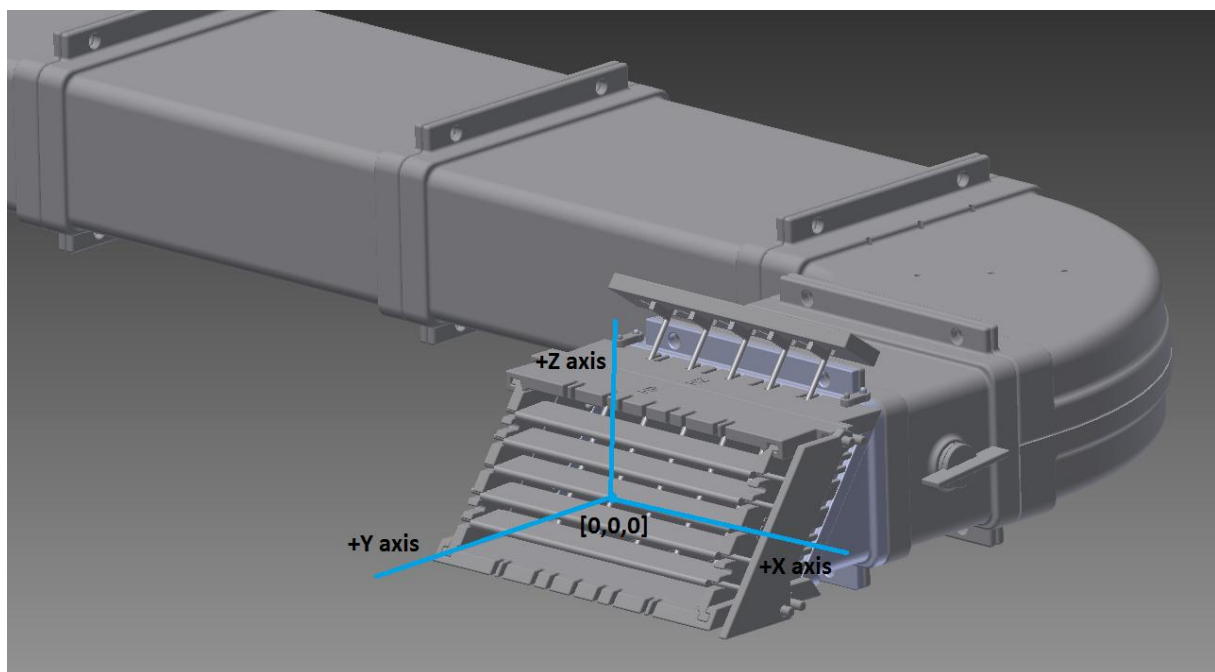


Figure 2.16 Zero point and coordinate system

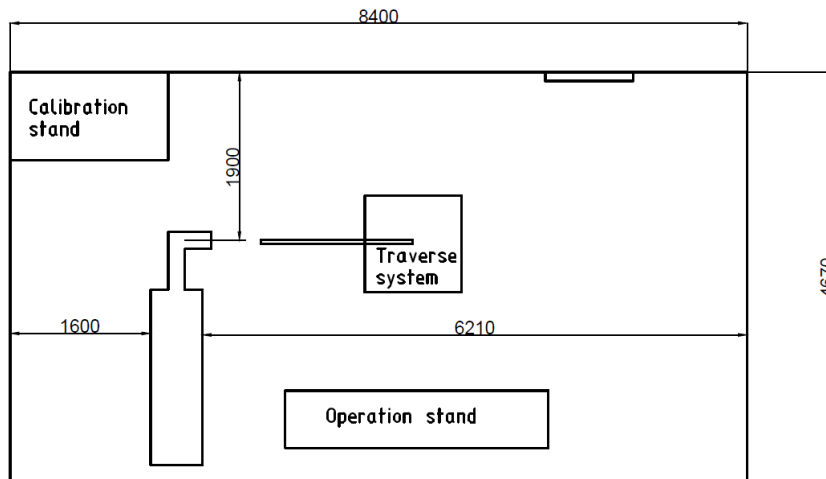
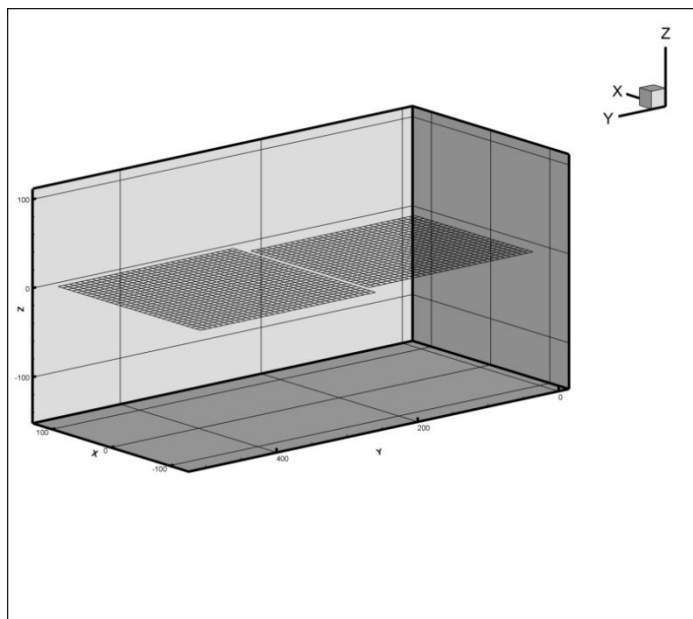


Figure 2.17 Location in laboratory

Schematic location of the air vent and traverse system is presented in Figure 2.17. The flow is meeting the condition of free air jet, as it is not adjoining any wall or surface.

2.5.3 Traverse grid description

The measurement of one point in the grid takes approximately 4-5 seconds. The traverse positioning itself takes around 2 seconds, it takes 2 seconds till the probe is not vibrating after moving and 1 second for measurement (the measurement is done with sampling frequency 1024 Hz). Traverse grids were created so that measurement of each grid would not take more than 1.5 hour (after the measurement of each grid, the probe needs to be re-calibrated).



“horiz1”

X=-100:8:100 (26 points)

Y=10:8:240 (30 points)

Z=const (depending of jet horizontal angle)

In total 780 points.

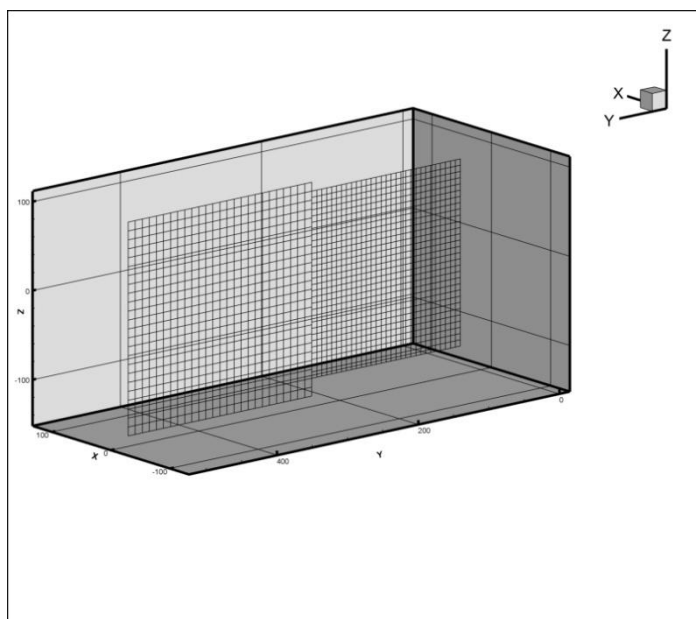
“horiz2”

X=-120:8:120 (31 points)

Y=250:8:498 (32 points)

Z= const (depending of jet horizontal angle)

In total 992 points.



“vert1”

X= const (depending of jet vertical angle)

Y=30:7:240 (31 points)

Z=-120:7:90 (31 points)

In total 961 points.

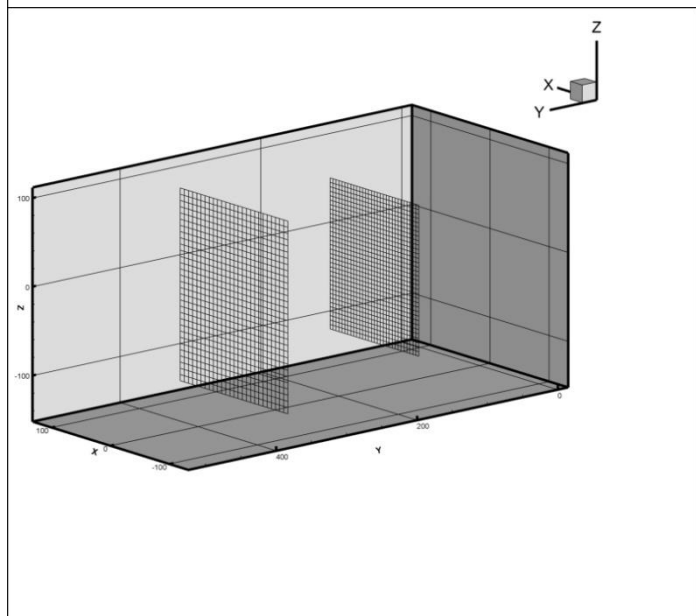
“vert2”

X= const (depending of jet vertical angle)

Y=240:10:500 (26 points)

Z=-140:10:100 (26 points)

In total 676 points.



“perp1”

X= -75:5:75 (31 points)

Y=150

Z= -100:5:70 (35 points)

In total 1086 points.

“perp2”

X= -90:7:92 (27 points)

Y=350

Z=-127:7:90 (32 points)

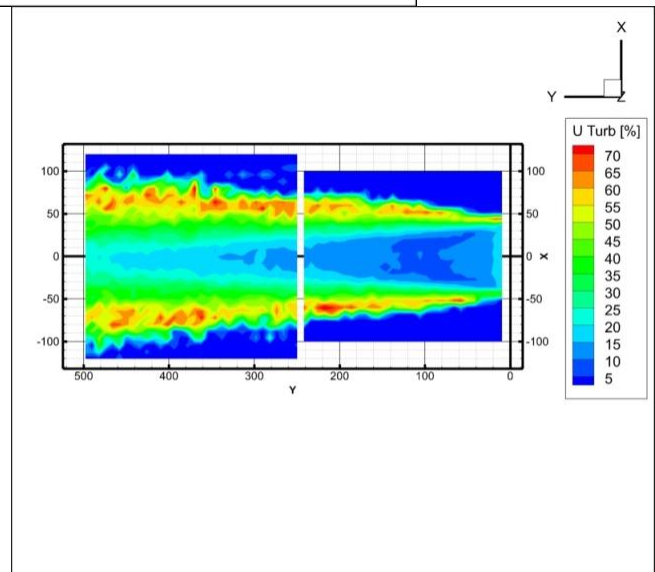
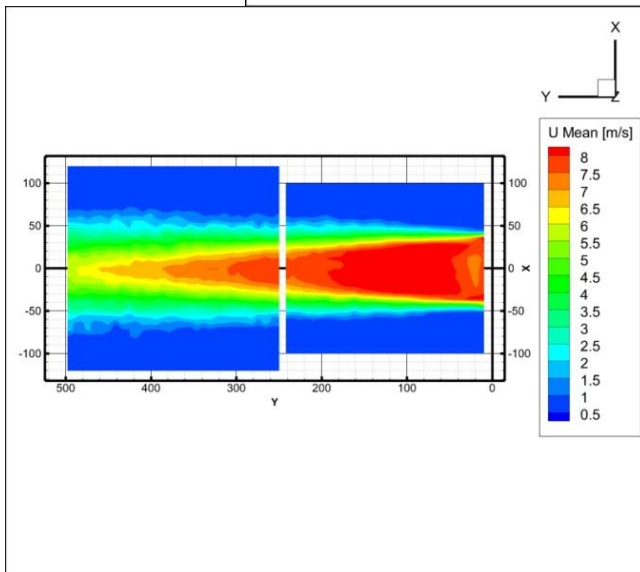
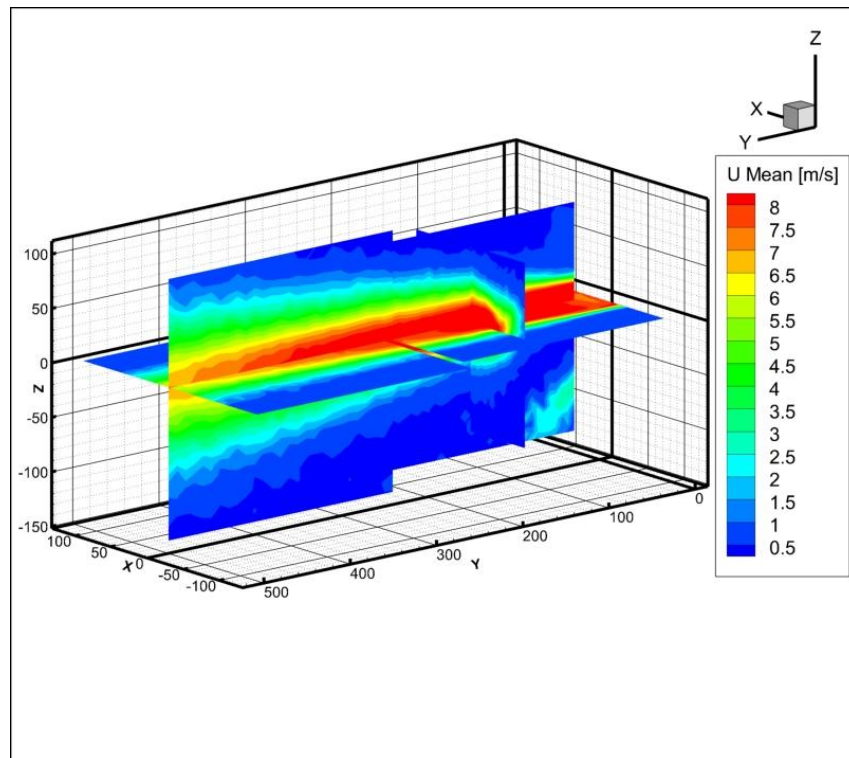
In total 864 points.

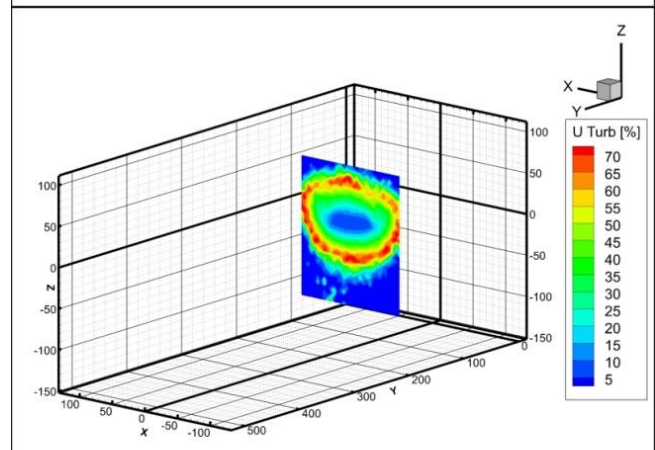
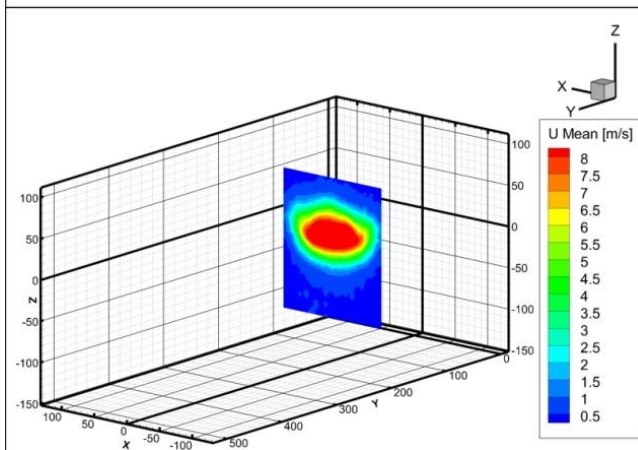
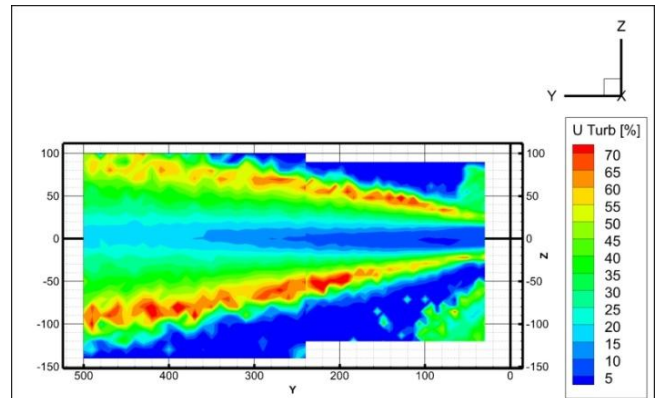
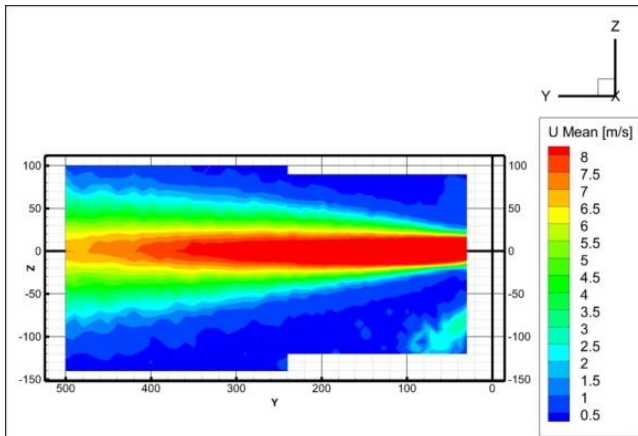
2.5.4 Evaluated cases

Based on previous research and experience of supervisor of this thesis and doc. Jedelský, there were 4 cases selected for further examination. Measurement of one plane takes approximately 1,5 hour (net time of 1 case measurement is then 9 hours), and ambient conditions are changing during this time, they are listed in corresponding data files.

All measurements were conducted during winter 2015, when the ambient temperature in laboratory was $16^{\circ}\text{C} \pm 1\text{K}$, barometric pressure was $98\text{kPa} \pm 1\text{kPa}$ and air humidity level $55 \pm 10\%$.

2.5.4.1 Flow rate $80,6 \text{ m}^3/\text{h}$, straight piping, without air flow rectifier

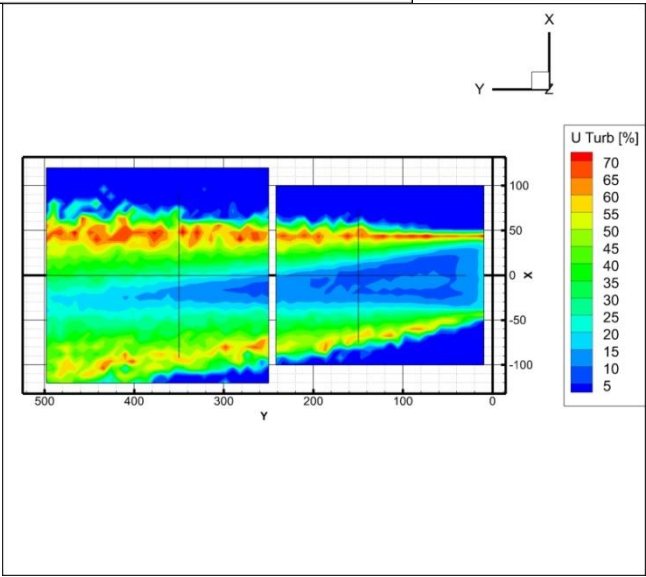
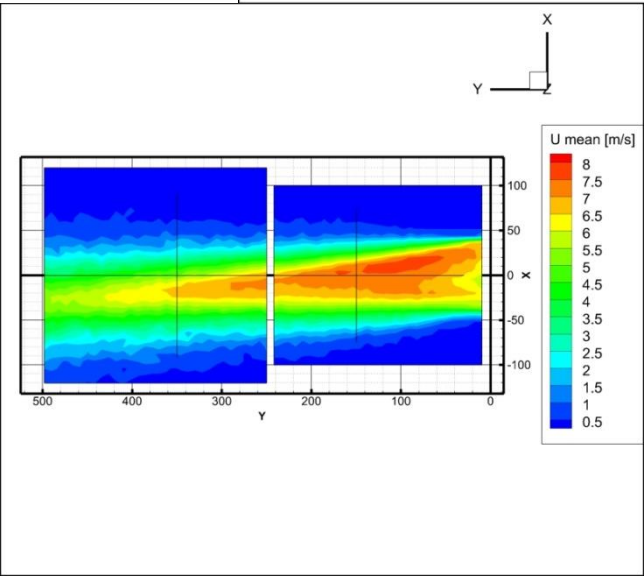
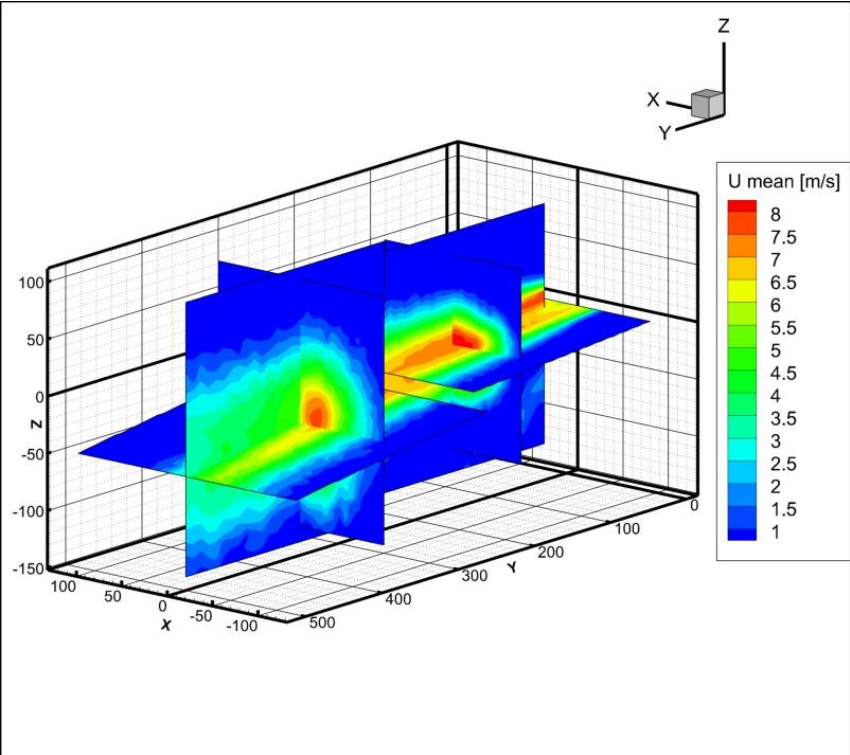


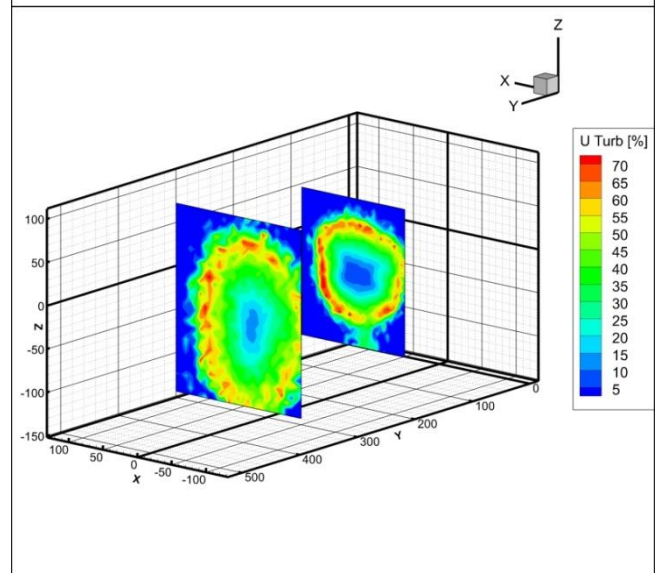
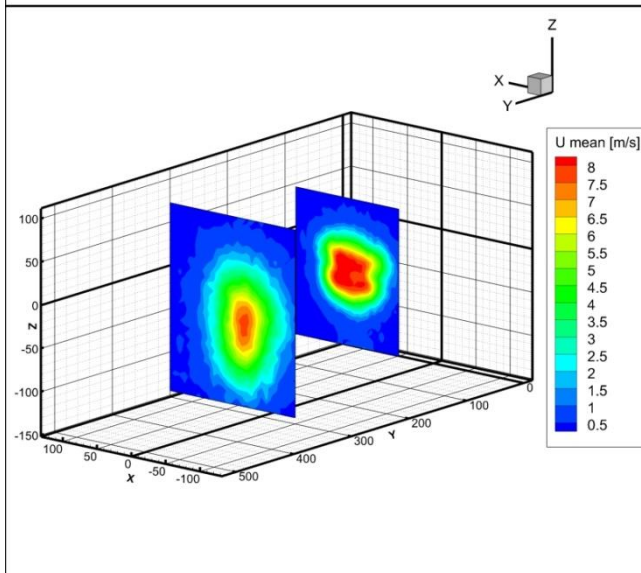
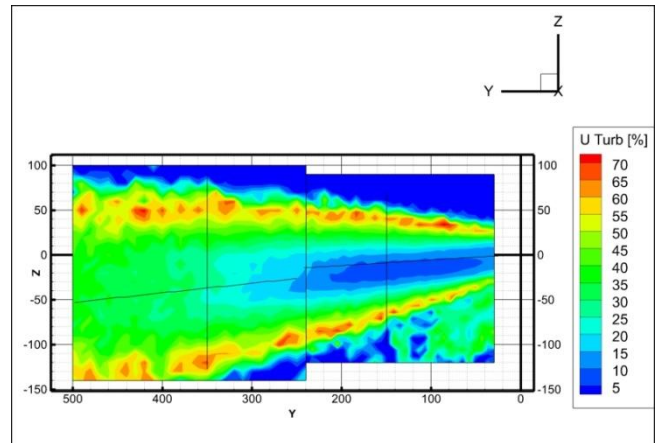
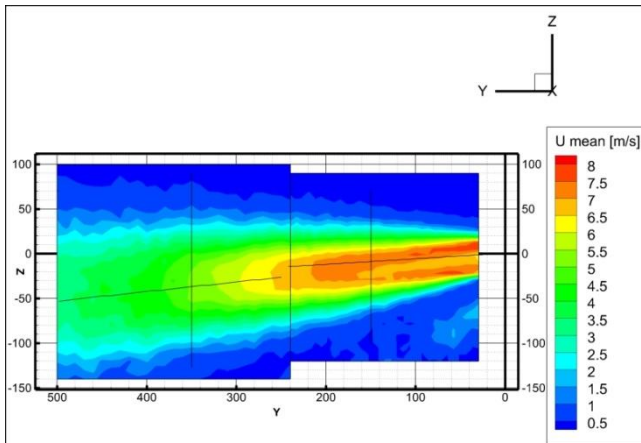


This measurement illustrates the problem with setting flow rate (that is dealt with hereafter) perfectly. For sake of clarity, same axis values are used on corresponding flow rates. Here, the maximal velocity is around 10% higher than in other cases. It points to be a systematical error. Nevertheless, the angular deviations from both axes are, even by visual control, nearly null.

The turbulence intensity and air velocity distribution is uniform as expected from straight piping.

2.5.4.2 Flow rate 80,6 m³/h, piping with bend, without air flow rectifier





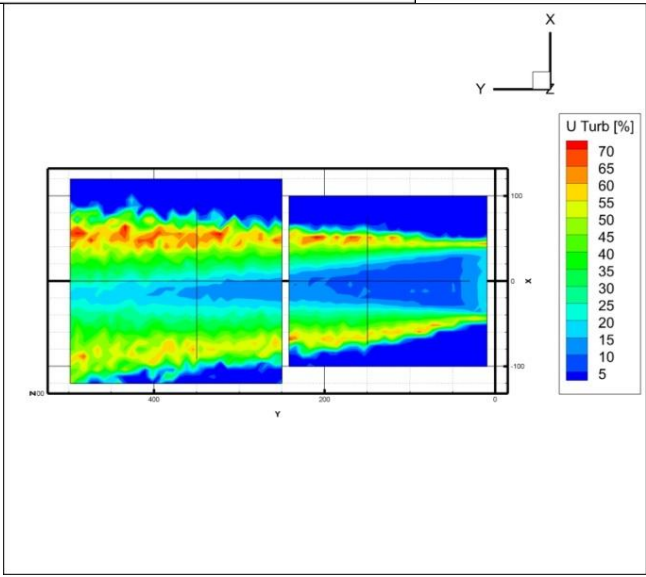
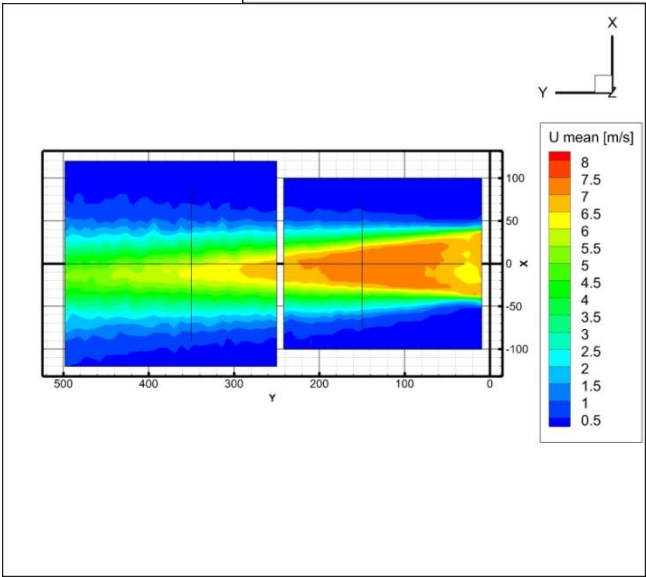
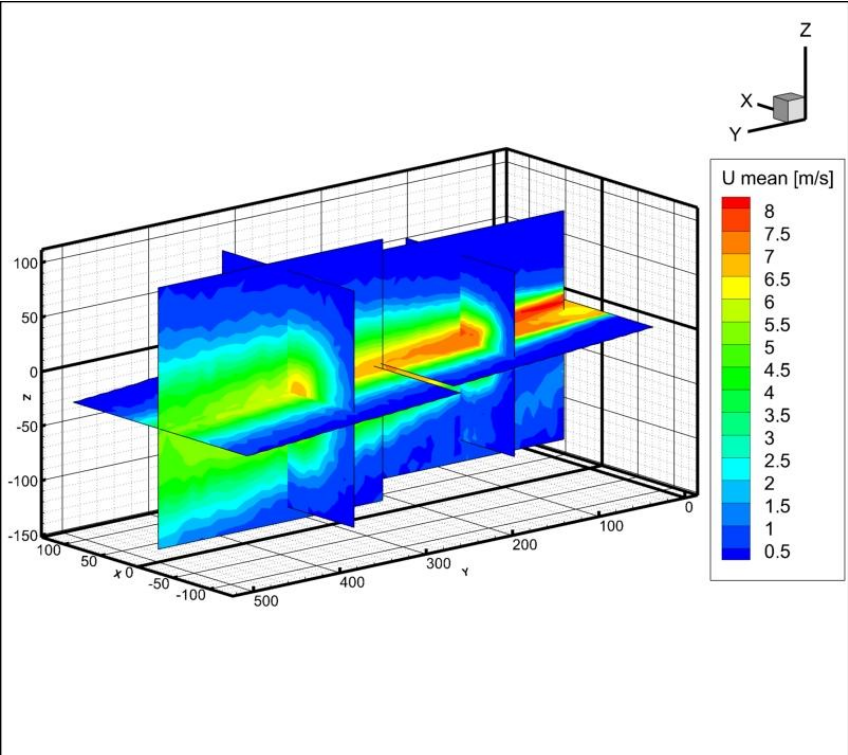
In the second evaluated case, we can see non uniform velocity distribution thanks to bend in test track, that is causing the air flow to bend as well. Horizontal and vertical angular deviations are visible.

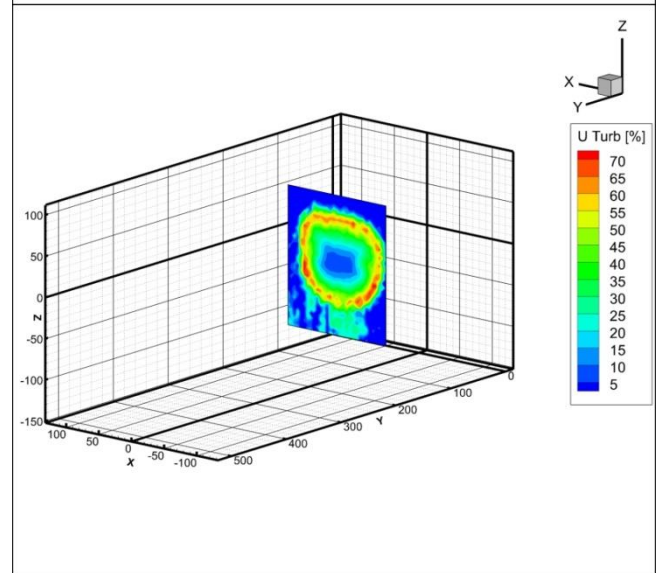
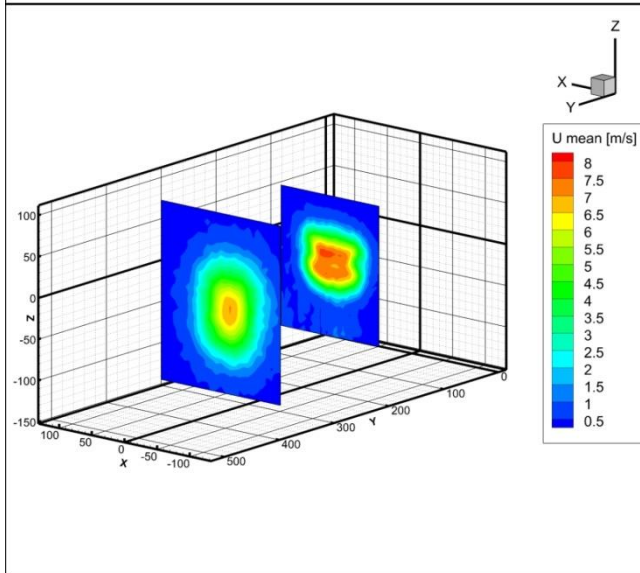
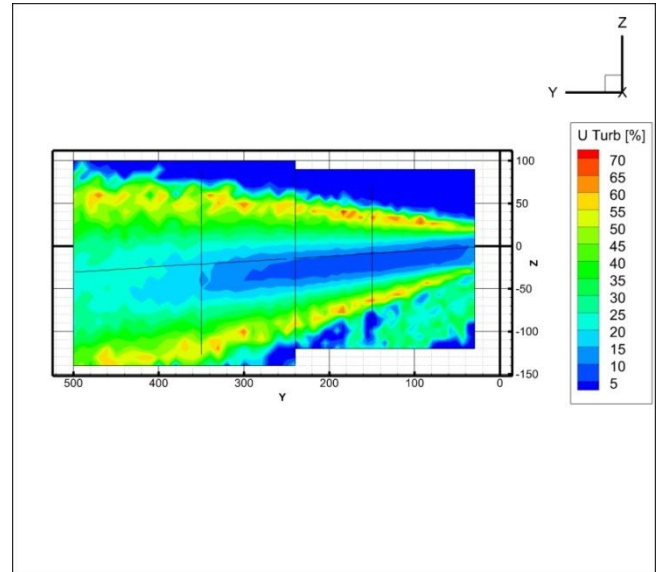
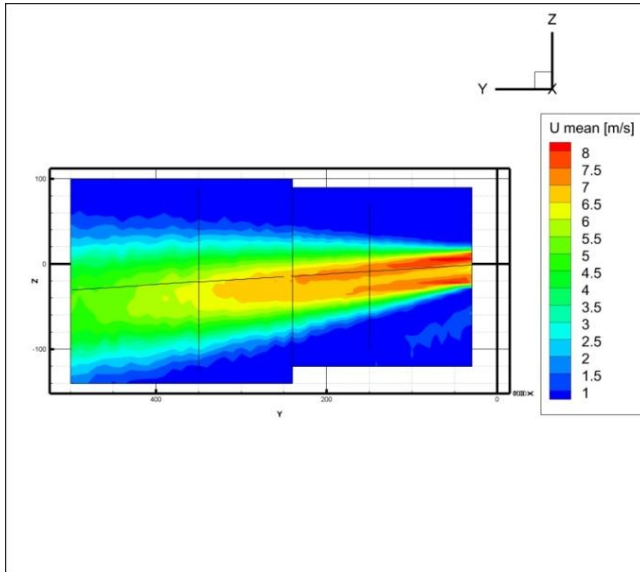
On XY plane, one can observe, that maximal velocity seem to be not at the vent outlet, which is not true. This inaccuracy can be seen also in other cases and is there thanks to wake region behind the central blade.

Also, what is visible here on rectangular (XZ) planes is that the shape of air jet is more alike rectangular opening near the vent, but with increasing distance from the vent, the air stream is becoming circular.

Turbulence in XZ plane is in this case (without air flow rectifier) not uniformly distributed, pointing at possible improvement.

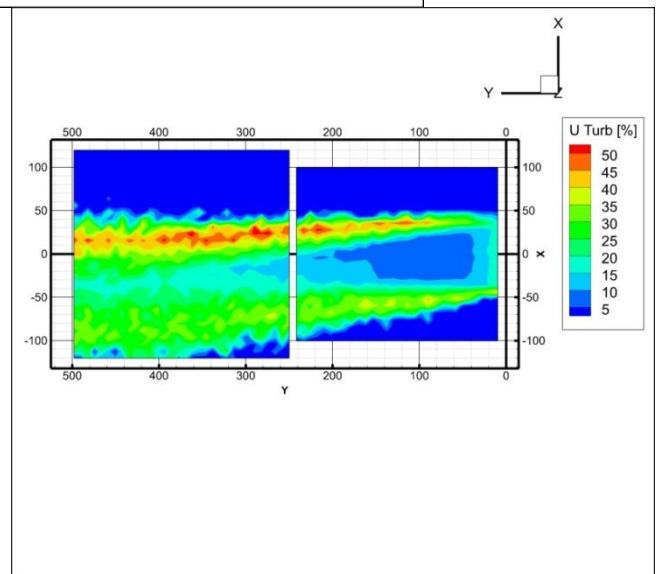
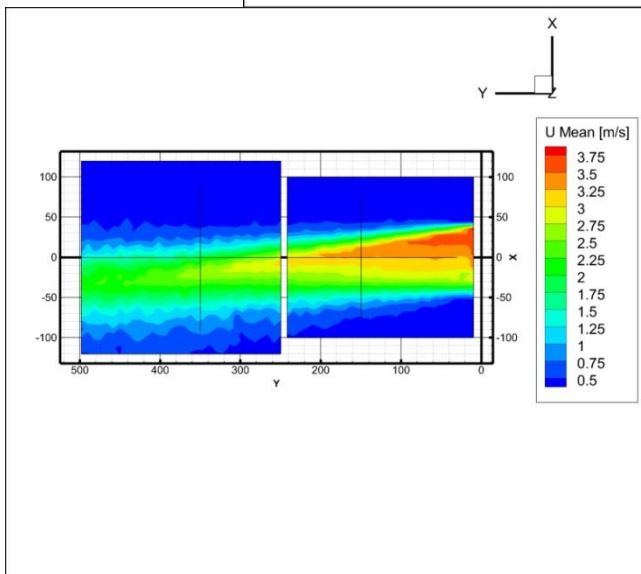
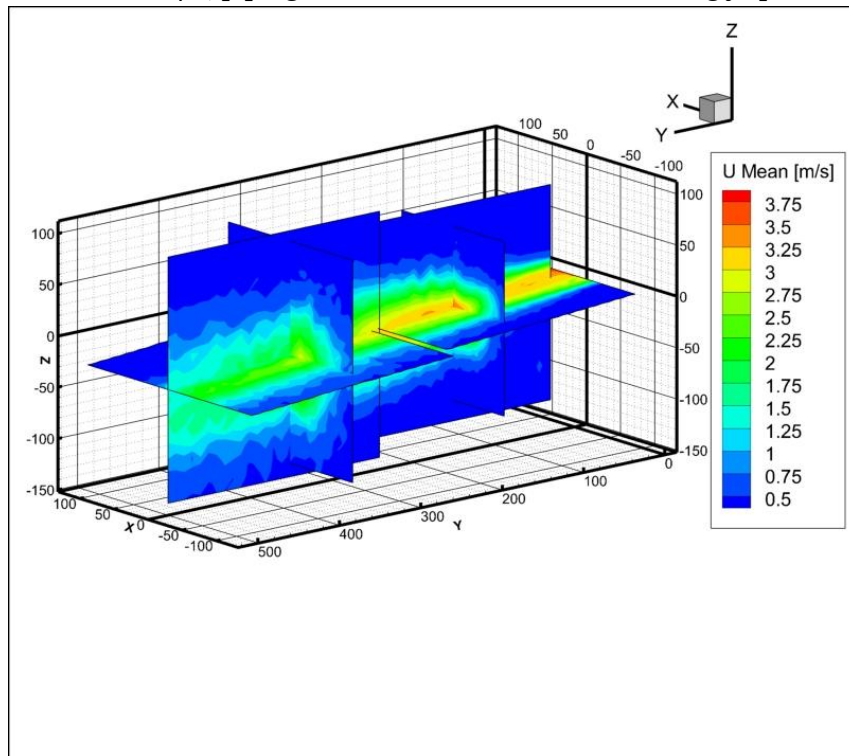
Flow rate 80,6 m³/h, with bend, with air flow rectifier

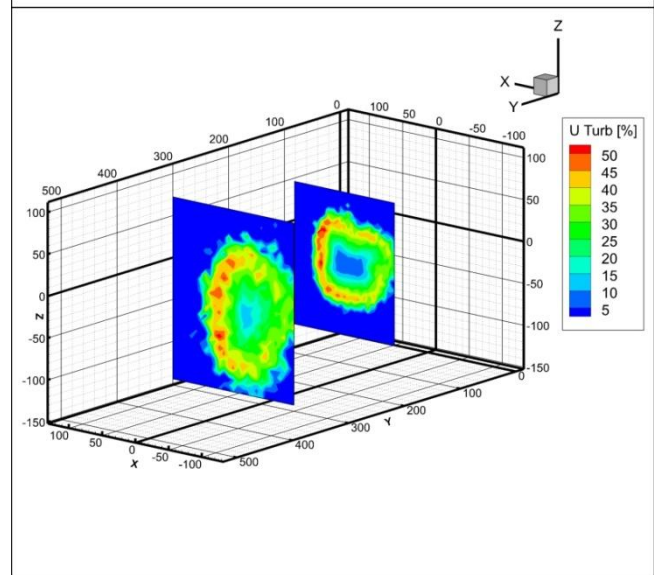
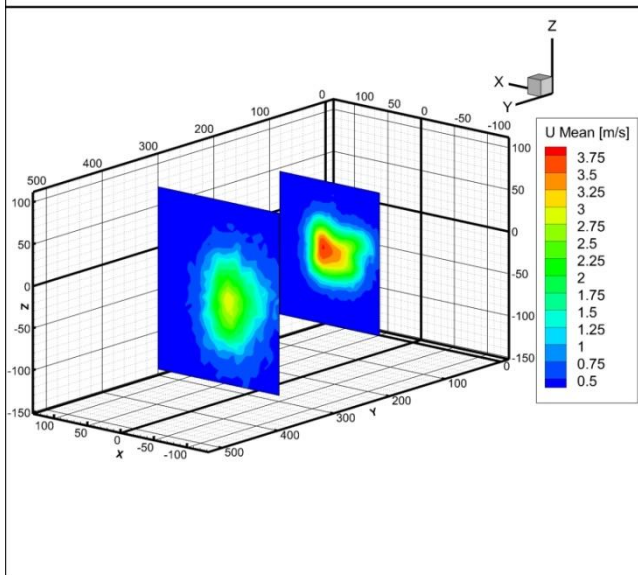
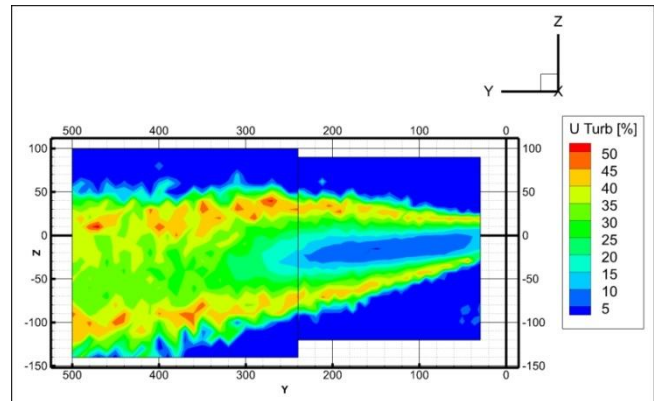
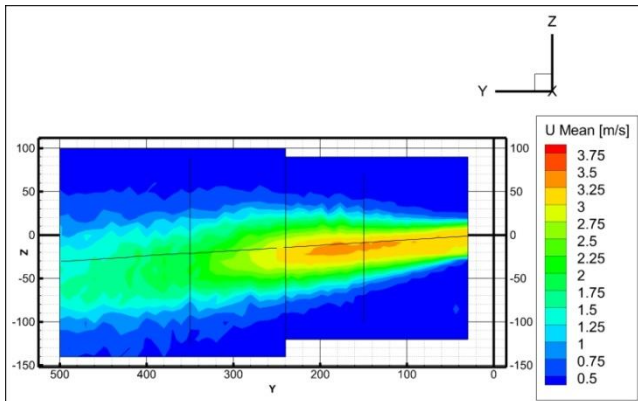




This case is specific in uniformly distributed turbulence intensity in XZ plane, thanks to air flow rectifier in bend, which is in opposite to similar case without such rectifier.

2.5.4.3 Flow rate $33,5 \text{ m}^3/\text{h}$, piping with bend and with double closing flap





The case with double flap and smaller air flow rate is illustrating for air velocity and turbulence intensity distribution in XZ planes.

2.5.5 General remarks

- In the first evaluated case (high flow rate, straight piping) there was a mistake made in the setting of flow rate or in the calibration of the probe, as the highest reached velocity was more than 15% higher than expected, thus resulting in distortion of images (color bars are the same for corresponding flow rates)
- Having no bend, only one measured case had nearly no horizontal deviation from axis compared to the cases with bend, thus we can assume that bend has an effect on flow vertical deviation.
- The air flow rectifier that was put into measuring track in third measurement presented had a positive effect on Turbulence intensity distribution which can be seen best in planes perp1 of cases 2) and 3)

2.6 Repeatability of measurement

Main concern here is the horizontal and vertical setting of blades, which used to be a problem in previous theses, because the blades were not stable and had no measurable orientation. (Ležovič 2011a)

In this thesis on the other hand, only straight setting of blades is evaluated, which is done manually. There was also a handle 3D printed (by Ing. Pech) to hold blades in place, so this issue was solved.

Apart from that, uncertainty of flow rate measurement is calculated hereafter to quantify the uncertainty. Apart from that, test measurement is done to quantify to uncertainty of flow rate setting, which is done by potentiometer controlling the fan power and secondary the flow rate. This is considered a first step in broader variety of actions taken to make the measurement more accurate and repeatable.

2.7 Spread Angles evaluation

2.7.1 Coordinate system and angles

Originally, in Master thesis of Ing. Ležovič there were only angles of flow border and flow axis determined, with coordinate system shown in Figure 2.18

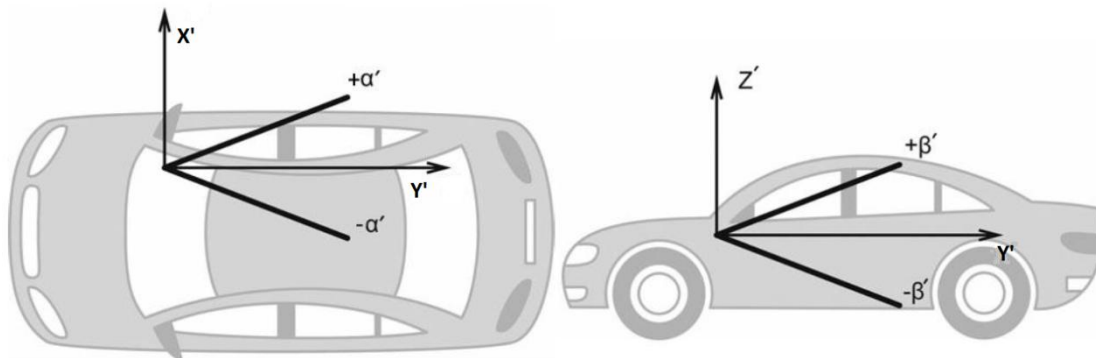


Figure 2.18 Coordinate system of vehicle (adjusted from (Ležovič et al. 2013/11/17))

Bc. Caletka in his Bachelor thesis further expanded these criteria (angles) by spread angle and these parameters will be used also in this thesis. The way the angles are defined can be seen in **Figure 2.19** and **Figure 2.20** (adjusted from (Caletka 2014))

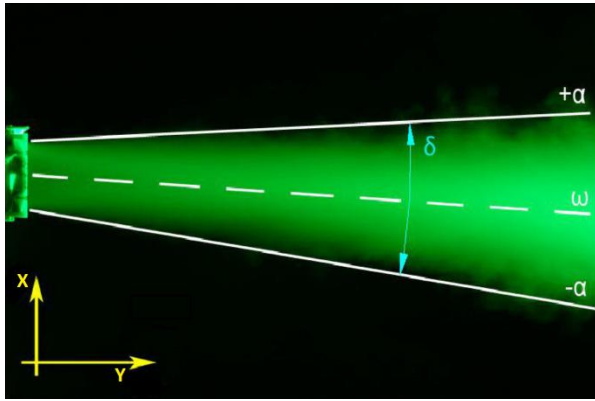


Figure 2.19 Vertical angles

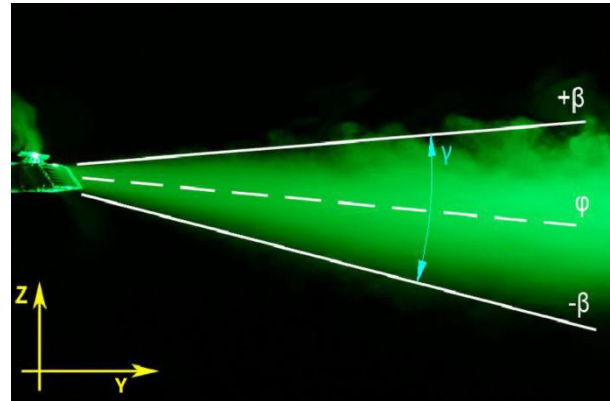


Figure 2.20 Horizontal angles

2.7.2 Data processing

Data processing by Ing. Lezovic was done using a computer program developed in Scilab software (flow borders recognition and spread angles evaluation). The lowest velocity he was able to calibrate the probe to was 1 m/s and the software was then searching for points with velocity in user specified interval (usually $<1;1,2> \text{ m/s}$), and then interpolating a line between them.

During measurements of this Master thesis, a new calibrator which the probe could be calibrated with for velocities as low as $0,5 \text{ m/s}$ was available. The new program for border recognition and angles evaluation was developed in commercially more used software MATLAB. As the syntax of Scilab and MATLAB is not compatible, it had to be developed from scratch.

Also, this program can be used for usual data display instead of Tecplot software which is available and used on Department of Thermomechanics and Environmental Engineering.

The advantage of this program is, that it can load even unsorted data from .xls files that are used for data export from Streamware (in opposite to loading data to Tecplot, where they need to be sorted by Z,Y and X dimension respectively). The measured grid is created automatically and all rows and columns are loaded. An algorithm is then searching for the highest value of velocity in a column and saving it. The border in such column is then the place in the grid where the velocity is 10% of axial (the maximal found) velocity.

In case of flow rate $33,5 \text{ m}^3/\text{h}$, 10% of axial velocity often is under $0,5 \text{ m/s}$, which is lowest calibrated velocity, so instead of 10% rule, 16% rule is applied.

This algorithm is run for each column and the border location data are then interpolated with a line and the angle deviation from horizontal/vertical axis is taken as a program output.

2.7.3 Software for border recognition outcome example

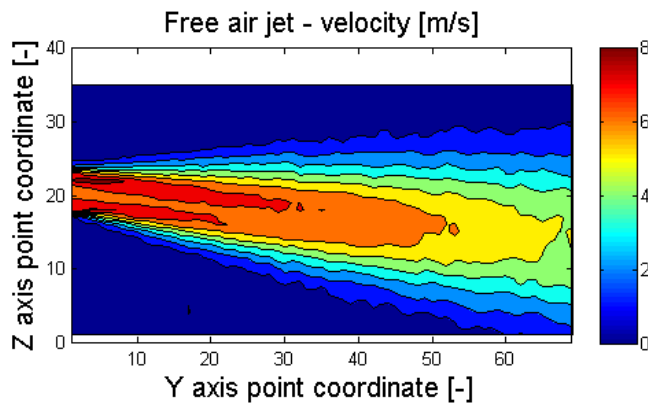


Figure 2.21 Velocity field

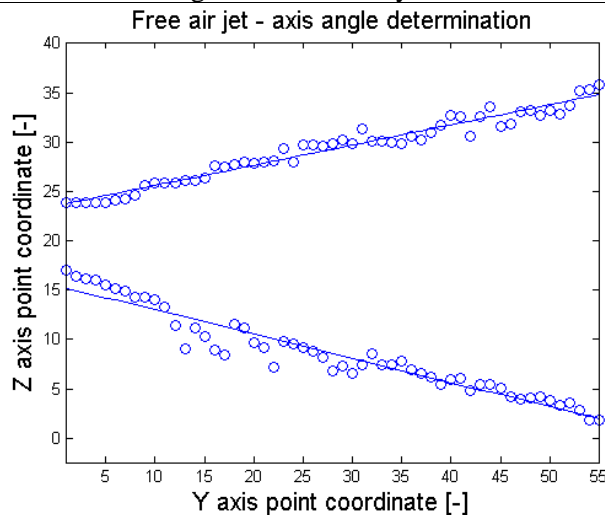


Figure 2.22 Flow border determination

Figure 2.21 and Figure 2.22 show the outcome of velocity field from developed program in MATLAB software, from which is the flow border determined.

In the velocity field figure, there are 69 columns visible, although in the next figure there are only 55 columns (Y axis coordinate). This is due to the fact, that the border is selected as a place with 10% of axial velocity in respective column but the lowest calibration velocity is 0,5 m/s, meaning the background in Figure 2.21 has value approx. 0.5. Thus when the axial velocity decreased below 5 m/s, the flow border is not determined.

The text output from program are then angles of both borders, aspread and an axis.

2.7.4 Angles evaluation

Horizontal angles

Flow rate	Case/Angle	$+\beta$ [°]	$-\beta$ [°]	φ [°]	γ [°]	K_s [-]
80,6 m ³ /h	Without flow rectifier, without bend	7,18	-8.9	-0,86	16,09	4,90
	Without flow rectifier, with bend	10,04	-13,86	-1,91	23,9	3,19
	With flow rectifier, with bend	11,4	-13,98	-1,28	25,38	2,98
33,5 m ³ /h	With double flap, with bend	6,36	-10,43	-2,03	16,79	4,68

Table 2.4 Horizontal angles

Vertical angles

Flow rate	Case/Angle	$+\alpha$ [°]	$-\alpha$ [°]	ω [°]	δ [°]	K_s [-]
-----------	------------	---------------	---------------	--------------	--------------	-----------

80,6 m ³ /h	Without flow rectifier, without bend	3,75	-1,74	1,01	5,5	14,67
	Without flow rectifier, with bend	6,14	-4,9	0,62	11,04	7,24
	With flow rectifier, with bend	2,32	-3,83	-0,76	6,16	13,09
33,5 m ³ /h	With double flap, with bend	3,96	-4,87	-0,46	8,83	9,1

Table 2.5 Vertical angles

Angles determined here are subject of comparison of smoke method visualization, which is conducted by Bc. Caletka, and evaluated in software Interfer (Caletka 2014) with various possible configurations. As the accuracy of HWA method is generally considered as high, the visualization method can be calibrated according to presented results.

2.8 CTA measurement uncertainty

Uncertainty of velocity measurement done by CTA is divided here to three subchapters

- HWA uncertainty
- Flow rate measurement uncertainty
- Flow rate setting uncertainty

2.8.1 Hot wire anemometry measurement uncertainty

Calculation done based on HWA – Practical Guide (Jørgensen 2002)

The relative standard uncertainty $u(y_i)$ is a function of the standard deviation of the input variance:

$$u(y_i) = \frac{1}{y_i} \cdot S \cdot \left(\frac{\Delta x_i}{k_i} \right)$$

where $S = \partial y_i / \partial x_i$ is the sensitivity factor and k_i is the coverage factor related to the distribution of the input variance (Gaussian, rectangular etc.).

As most engineering applications are assumed to have a Gaussian error distribution, the 95% confidence level normally required is achieved by multiplying the standard uncertainty with the coverage factor $k=2$. The total relative expanded uncertainty then becomes:

$$U(tot) = 2 \cdot \sqrt{\sum u(y_i)^2}$$

Uncertainty of a single velocity sample acquired via an A/D board from a CAT anemometer with a single sensor probe. The uncertainty of each individual velocity sample is determined by non-statistical means based on detailed knowledge about the *instrumentation, calibration equipment and experimental conditions*. The uncertainties presented below are *relative standard* uncertainties. (Jørgensen 2002)

Velocity sample uncertainty

Source of uncertainty	Input variants	Input Value	Relative output variants	Relative standard uncertainty
	Δx_i	Δx_i	$\frac{1}{U} \cdot \Delta y_i$	$\frac{1}{k} \cdot \frac{1}{U} \cdot \Delta y_i$
Calibrator	ΔU_{cal}	1%	$U(U_{cal}) = \frac{1}{100} \cdot STDV(U_{calibrator}(\%))$	0.01
Linearisation	ΔU_{fit}	0.5%	$U(U_{lin}) = \frac{1}{100} \cdot STDV(\Delta U_{lin}(\%))$	0.005
A/D resolution	E_{AD} n	21 volts 32 bit	$U(U_{res}) = \frac{1}{\sqrt{3}} \cdot \frac{1}{U} \cdot \frac{E_{AD}}{2^n} \cdot \frac{\partial U}{\partial E}$	0,00000121
Probe positioning	θ	1 °	$U(U_{pos}) = \frac{1}{\sqrt{3}} \cdot (1 - \cos \theta)$	0,00009
Temperature variations of wire	A B $T_w - T_o$ ΔT	1,396 0,895 200 °C 4 °C	$\frac{1}{U} \cdot \frac{\Delta T}{(T_w - T_o)} \cdot \left(\frac{A}{B} \cdot U^{-0,5} + 1 \right)$	0,0018
Temperature variations of ambient air	ΔT	4 °C	$U(U_{\rho,T}) = \frac{1}{\sqrt{3}} \cdot \Delta \rho_{,T} = \frac{1}{\sqrt{3}} \cdot \frac{\Delta T}{273}$	0.0085
Ambient pressure	ΔP	10 kPa	$U(U_{\rho,P}) = \frac{1}{\sqrt{3}} \cdot \left(\frac{P_0}{P_0 + \Delta P} \right)$	0.006
Humidity	ΔP_{wv}	1 kPa	$U(U_{hum}) = \frac{1}{\sqrt{3}} \cdot \frac{1}{U} \cdot \frac{\partial U}{\partial P_{wv}} \cdot \Delta P_{wv}$	≈0

Table 2.6 Velocity sample uncertainty

$$u_{HWA} = 2 \cdot \sqrt{\sum u(y_i)^2} = 3,076\%$$

Is the total uncertainty for air velocity $10 \frac{m}{s}$.

The greatest influence is from air calibrator (the automatic calibrator uncertainty is ½ of classical calibrator).

In comparison to previous test track uncertainty calculation by Dr. Lizal (Lizal 2007) and due to new components of test track, uncertainty had decreased from 7,7% to 3,076%. This is although only theoretical, as he was taking into account also uncertainty from neglecting 3. Component of velocity (his measurement was done with 2 wire probe), so the uncertainty values are not comparable.

2.8.2 Flow rate measurement uncertainty

Flow rate measurement and setting is done according to standard ČSN EN ISO 5167-2 (with orifice plate)

The equation

(2.2) determining the flow rate is expressed in above mentioned ISO standard (ČNI 2003).

$$q_m = C \cdot \varepsilon \cdot \frac{\pi}{4} \cdot d^2 \cdot \frac{\sqrt{2\Delta p \rho_1}}{\sqrt{1 - \beta^4}} \quad (2.2)$$

Where q_m is the mass flow rate

C is the flow rate coefficient

d is the orifice diameter

Δp is the pressure difference

ρ_1 is the air density

β is the ratio of orifice and piping diameter

According to chapter 8.2.1.3 in ČSN EN ISO 5167-1, only uncertainty of $\varepsilon, d, D, \Delta p, \rho_1$ need to be taken into account.

The uncertainty of such measurement can be calculated according to Equation

(2.3) (ČNI 2003)

$$\frac{\delta q_m}{q_m} = \sqrt{\left(\frac{\delta C}{C}\right)^2 + \left(\frac{\delta \varepsilon}{\varepsilon}\right)^2 + \left(\frac{2\beta^4}{1 - \beta^4}\right)^2 + \left(\frac{\delta D}{D}\right)^2 + \left(\frac{2}{1 - \beta^4}\right)^2 + \left(\frac{\delta d}{d}\right)^2 + \frac{1}{4}\left(\frac{\delta \Delta p}{\Delta p}\right)^2 + \frac{1}{4}\left(\frac{\delta \rho_1}{\rho_1}\right)^2} \quad (2.3)$$

Where $\beta = \frac{d}{D} = \frac{46,493}{70,3} = 0,6614$

Uncertainty of flow rate coefficient

$(0,7 - \beta)\%$ — — — for $0,1 \leq \beta < 0,2$

$0,5\%$ — — — for $0,2 \leq \beta \leq 0,6$

$(1,667 \cdot \beta - 0,5)\%$ — — — for $0,6 < \beta \leq 0,75$ (ČNI 2003)

Selected value $\frac{\delta c}{c} = 0,5\%$

Uncertainty of piping dimension

$$\frac{\delta D}{D} = 0,3\%$$

Recommended value from (ČNI 2003).

Uncertainty of expansion coefficient

$$\frac{\delta \varepsilon}{\varepsilon} = 3,5 \frac{\Delta p}{\kappa \cdot p_1} = 3,5 \frac{274}{1,4 \cdot 205} = 3,341\% \text{ (from (ČNI 2003))}$$

$\Delta p, \kappa, p_1$ values taken and averaged from Labview program, that was developer for real time data display and logging.

Uncertainty of orifice dimension

$$\frac{\delta d}{d} = 0,05\%$$

Recommended value from (ČNI 2003).

Uncertainty of pressure difference measurement

$$\frac{\delta \Delta p}{\Delta p} = 0,92\%$$

Value specified in product specification of measuring device (Airflow volume velocity transducer PTSXR) is 0,5% from range of measuring device, in our case then 0,92%)

Uncertainty of density measurement

And for calculation of density uncertainty, we need to derive required equations, as density is computed by Labview program from below mentioned Equation (2.4):

$$\rho = \frac{p}{r \cdot T} \quad (2.4)$$

For case of simplicity we, will use above mentioned equation, even though the program is more complicated, as it is taking into account also air humidity and its effect on air density. According to recommendations in (ČNI 2003) for technical measurements, we neglect this effect.

For uncertainty of measurement we further need derivatives of the Equation (2.4).

$$u_{B\rho} = \sqrt{\left(\frac{\delta \rho}{\delta p} \cdot u_{Bp}\right)^2 + \left(\frac{\delta \rho}{\delta T} \cdot u_{BT}\right)^2} \quad (2.5)$$

$$\frac{\delta \rho}{\delta p} = \frac{1}{r \cdot T} \quad (2.6)$$

$$\frac{\delta \rho}{\delta T} = -\frac{p}{r \cdot T^2} \quad (2.7)$$

And values of u_{Bp} , u_{BT}

$$u_{Bp} = 2,5 \text{ Pa (Airflow_Lufttechnik_GmbH 2015)}$$

$$u_{BT} = 0,3^\circ\text{C (Konečný 2011)}$$

And density uncertainty is then determined according to Equation (2.5) (air density from program Vlhky vzduch 3.0 (Pavelek 2010)):

$$u_{B\rho} = 0,000369$$

$$\frac{\delta \rho_1}{\Delta \rho_1} = \frac{0,000369}{1,1596} = 0,000318\%$$

With knowing all single values, we can then compute $\frac{\delta q_m}{q_m}$ according to Equation (2.3).

$$\text{Thus } \frac{\delta q_m}{q_m} = 3,413\%$$

In our application, we are dealing with volumetric flow rate q_v (instead of mass flow rate q_m in equation (2.3)), the volumetric flow rate is determined according to Equation (2.8).

$$q_v = \frac{q_m}{\rho} \quad (2.8)$$

As the uncertainty of density is very low, we can assume, that

$$\frac{\delta q_m}{q_m} \approx \frac{\delta q_v}{q_v} = 3,413\%$$

2.8.3 Flow rate setting uncertainty

As described in previous chapter, flow rate measurement was done according to standard ČSN EN ISO 5167, with one set variable being fan power. The power was set by potentiometer on electric power supply, which was not very precise.

Therefore, after agreement with supervisor of this thesis, uncertainty of setting this value will be calculated.

There were 15 measurements done from zero flow rate to $80,6 \text{ m}^3/\text{h}$ and the final value was written down.

Measurement number	$Q_i [\text{m}^3/\text{h}]$	Measurement number	$Q_i [\text{m}^3/\text{h}]$
1	81,10283	9	80,81718
2	79,50675	10	80,04837
3	79,533	11	81,91213
4	80,21993	12	79,09712
5	80,81885	13	80,90918

6	81,04552	14	79,95162
7	79,50898	15	81,98162
8	81,08604		
Average	80,50261		

Type A uncertainty evaluation is done according to equation (2.9) (Palenčár et al. 2001).

$$U_A(x) = s_{\bar{x}} = \frac{s_x}{\sqrt{n}} = \sqrt{\frac{1}{n(n-1)} \sum_{i=1}^n (x_i - \bar{x})^2} = \mathbf{0,230 [m^3/h]} \quad (2.9)$$

2.8.4 Uncertainties summary

In our case

$$\frac{\delta q_V}{q_V} = 3,413\% \approx 2,751 [m^3/h] = U_B(x)$$

We can further sum uncertainties of flow rate setting and measurement

$$U_C(x) = \sqrt{U_A(x)^2 + U_B(x)^2}$$

$$\mathbf{U_C(x) = 2,761 [m^3/h]}$$

Uncertainty of HWA is from above mentioned calculation.

$$u_{HWA} = 3,076\%$$

2.9 Issues encountered

2.9.1 Measurement in piping

Due to lack of jig, the insertion of probe into piping was done manually. The hole diameter being only 2,5 mm bigger than the greatest dimension of probe, it was rather hard to do so, and one probe was unfortunately destroyed during such operation. As the probe is rather expensive (approx. €500), it is advised to either drill bigger holes or use a custom made jig for insertion.

2.9.2 Air filtration

(Brunn 1995) recommends to incorporate air filter to test track for prolonging the lifespan and accuracy of probe measurement. In our case, the air flow filter is only part of calibration track, but not measuring track itself.

As the same track is also used for smoke method visualization, and smoke is generated from oil-like liquid, that is afterwards partially condensing in piping and staying there, it is advised to dismantle and clean the track before HWA measurement.

2.9.3 1 wire probe – shear layer flow

With 1 wire probe, one is measuring voltage that is proportional to heat transfer rate from wire. Problem is that is not direction-sensitive. With 2 or 3 wires, directional calibration is possible so that 3 components of velocity are measurable.

In shear layer flow, where even reverse flow is possible this becomes a serious problem, as we cannot distinguish the direction of flow. It is then advisable to measure flow at specific point with 2 or 3 wires song to confirm this assumption and eventually adjust flow border determination algorithm.

2.9.4 Wrong data reduction

In two cases, there were inexplicable mistakes in data (probably during data reduction). Both are shown underneath in

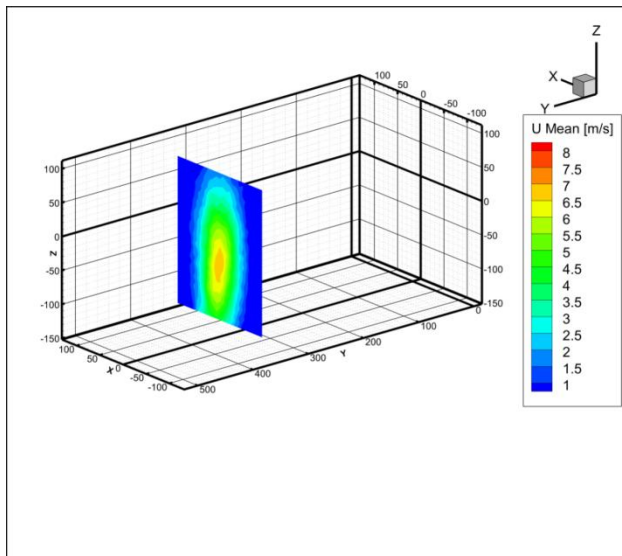


Figure 2.23 Error in data 1

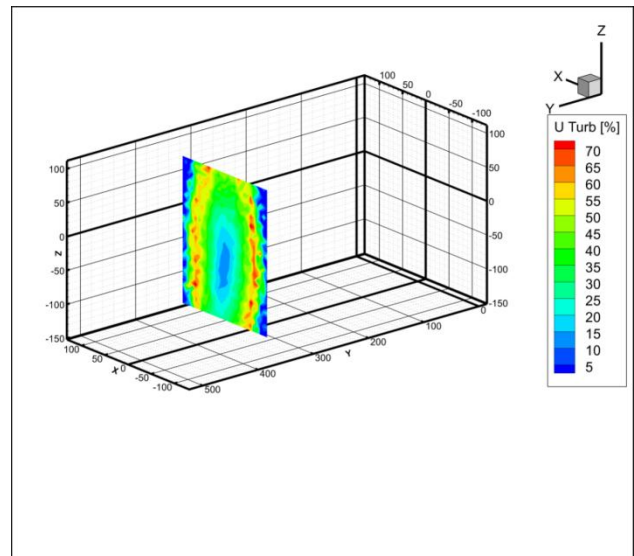


Figure 2.24 Error in data 2

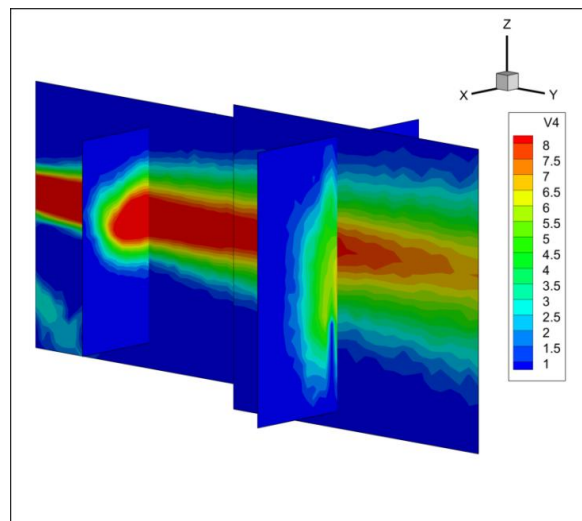


Figure 2.25 Error in data 3

3 Computational fluid dynamics simulation

Computational fluid dynamics (CFD) simulation is a fluid dynamics branch that is using computational power to solve Navier-Stokes equations (generally in 1,2 or 3 dimensions). As stated, the CFD simulation is not the main part of this thesis so only a brief explanation follows. It was conducted as a semestral work for the subject "Počítačové modelování II" with supervision of our lecturer, Ing. Jaroslav Volavý, PhD.

3.1 Fundamental equations

There are three types of fundamental equations used.

3.1.1 Continuity equation

Here, the assumption is, that mass cannot be either created or destroyed. The continuity equation (Honus 2014):

$$\frac{\delta \rho}{\delta t} + \nabla \cdot (\rho \cdot \vec{v}) = 0 \quad (3.1)$$

Where ρ is the fluid density

t is time

\vec{v} is the element velocity vector

∇ is the Nabla operator

3.1.2 Momentum equation

From Newton's second law:

$$\vec{F} = m \cdot \vec{a} \quad (3.2)$$

Where \vec{F} is the force on elementary volume,

m is the weight of elementary volume and

\vec{a} , which is the acceleration of elementary volume.

This can be further rewritten as famous Navier-Stokes equations.

3.1.3 Energy equations

In case of an incompressible medium, it can only be computed with the continuity and momentum equations. In case it is necessary to compute a process where the fluid compressibility has a significant role, it is needed to consider also energy dissipation. This is verbally formulated in the first law of thermodynamics: "Energy can be neither created nor destroyed, it can only change in form". (Volavý 2015)

Altogether there are 5 equations (3 momentum equations for 3 dimensional cases) and 5 unknowns – 3 velocities, pressure and temperature at each point. Equation of state can further be added to compute

above-mentioned temperature. Unfortunately there is no general solution for such problems. Mathematical methods with iterative processes have to be used to estimate the missing variables. (Volavý 2015)

3.2 Physical modeling workflow

During the pre-processing stage, it is necessary to consider following:

- What are we to model?
- What is the expected result?
- In what way we will present the outcomes?

From the modeled case:

- Is the flow steady or unsteady?
- Which phenomena can we neglect and which we cannot?
- How can we simplify the case and what influence will it have on results?

And apart from these, there are simulation conditions

- How much time do we have?
- How much computational power do we have?

The proposed solution is usually a compromise, due to the need of prioritization in above-mentioned aspects.

In a preprocessing part, the geometry of the modeled case, computational mesh and mathematical models were prepared and used to compute unknown variables.

Processing

The simulation was initialized and the residuals were checked – in case their values were falling constantly, rising or periodically changing that would have been an indicator of possible error in settings or invalid assumption. (Volavý 2015)

Post-processing

In this section, results are displayed in the desired form (table, figure, etc.)

3.3 Pre-processing

The case simulated is the higher flow rate ($80,6 \text{ m}^3/h$) without air flow rectifier with bend.

The air vent was printed on 3D printer, accurate 3D CAD model was available for the measurement. The simplification of the complicated set of parts was nearly impossible with Surface Repair tools in STAR-CCM+, the decision was made to remodel it. The CAD model was created in Autodesk Inventor, version 2013, saved to .stp data type and imported to Star-CCM - Figure 3.1.

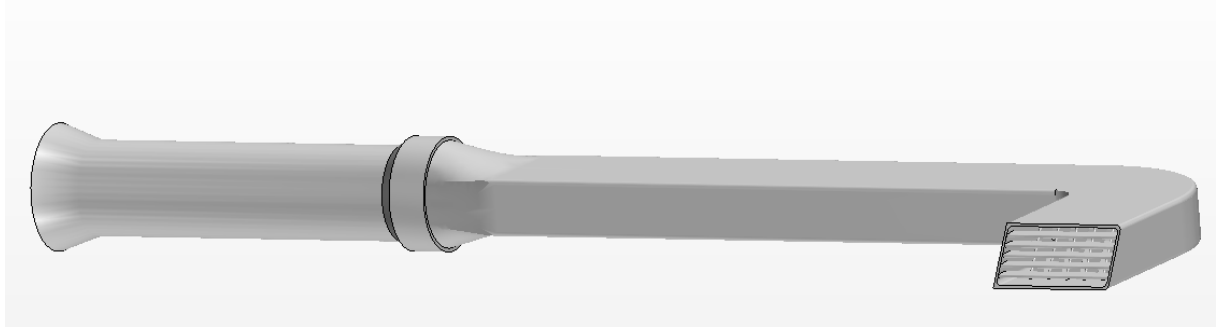


Figure 3.1 Imported air vent with piping

In order to successfully run the simulation, it was necessary to repair the surfaces (damaged during creation and vent import). Complications occurred with Surface Repair tool in Star-CCM, and also while getting a “negative” – the air domain so different software – ANSYS Fluent – was used.

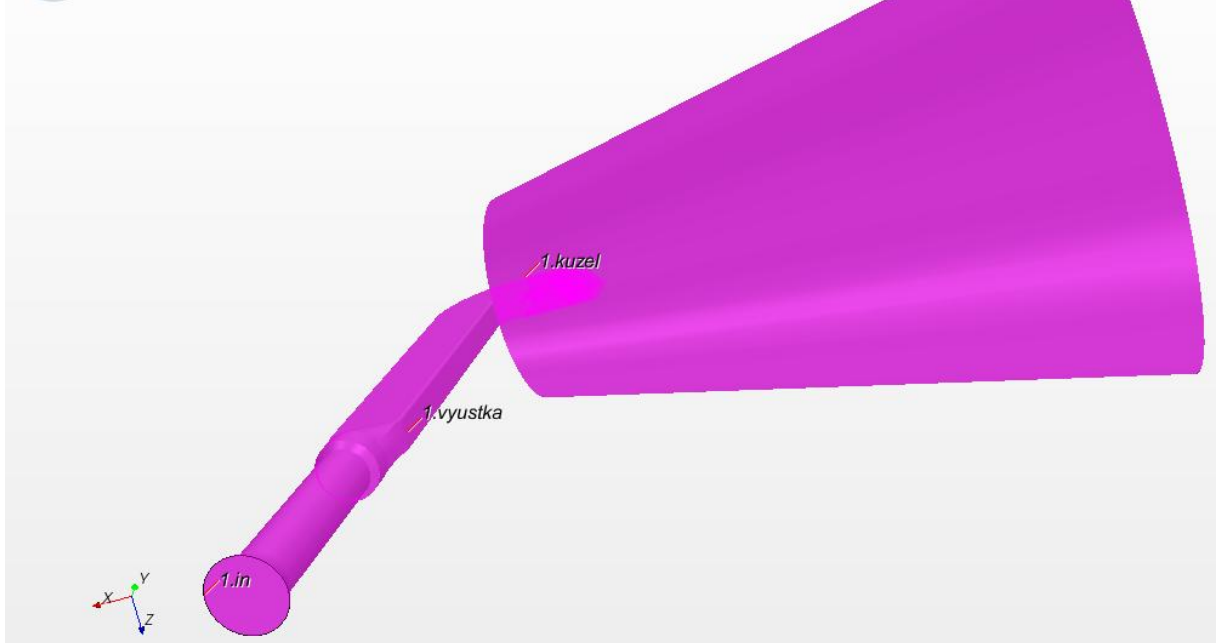


Figure 3.2 The air vent with defined regions

On Figure 3.2 we can see the imported vent with defined regions is presented

1. “In” – boundary condition “velocity inlet” used
2. “Vyustka” – boundary condition “wall” used
3. “Kuzel” – boundary condition “pressure outlet” used

There were created separate regions for blades and closing flap as well in order to be able to refine the generated mesh.

Mesh was generated with parameters seen in Table 3.1

Used model	Polyhedral mesher
Base size	0,03 m
Prism layer mesher	5 layers, stretching 1.5, thickness 20% relatively
Surface remesher	

Table 3.1 Mesh properties

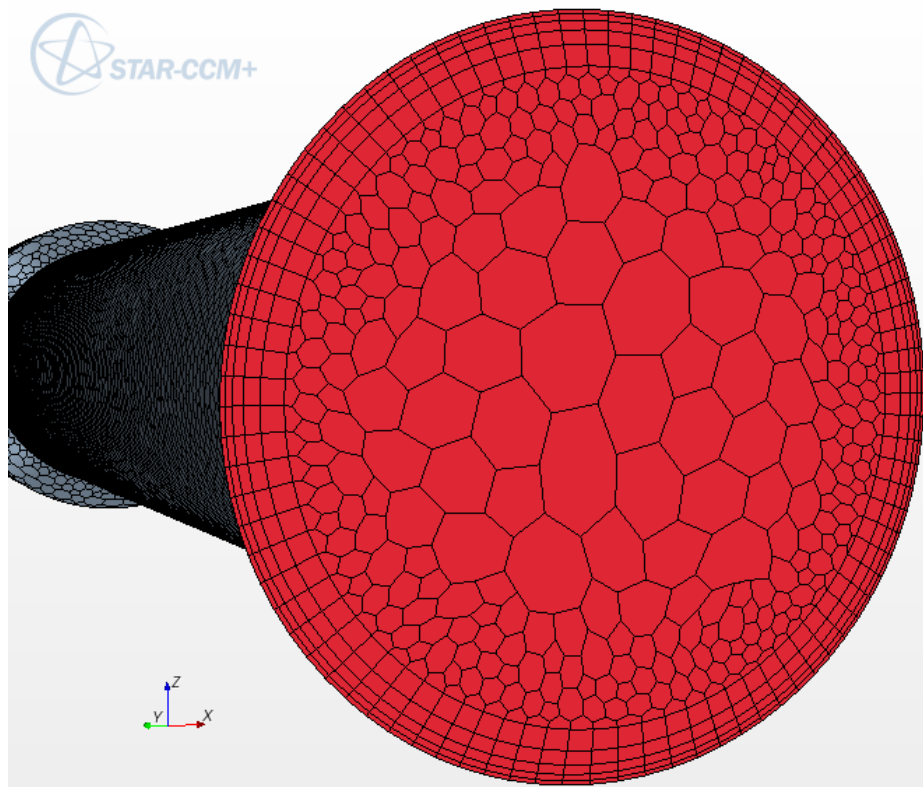


Figure 3.3 Entry region mesh detail

In Figure 3.3 entry region is shown. For more precise meshing, surface curvature (points that define circle) was set to value 72 (default 36) and around closing flap and blades there was another prism layer made, as can be seen in Figure 3.4

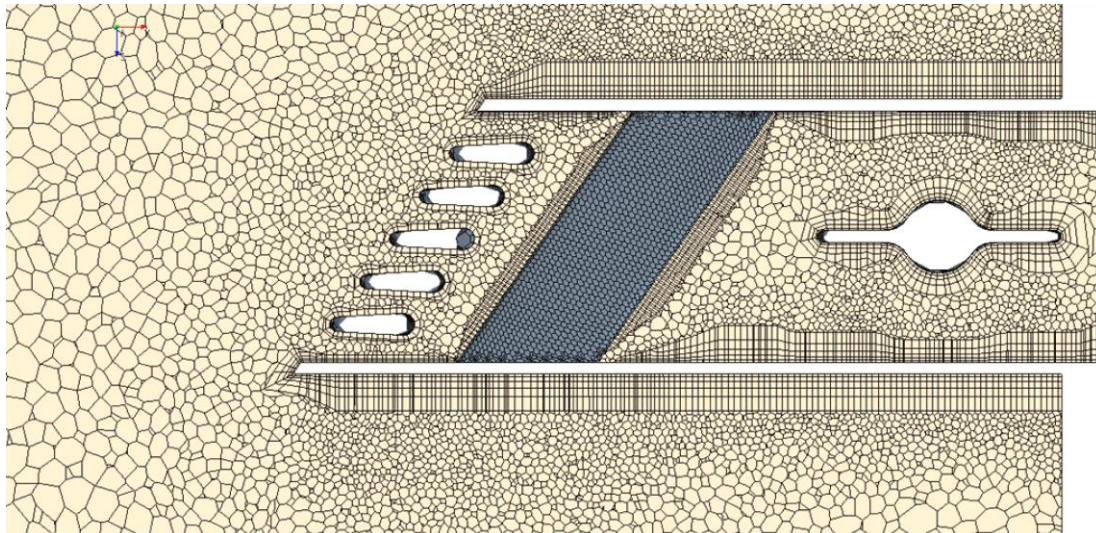


Figure 3.4 Prism layer around blades and closing flap

For more accurate solution of vent outlet, there was a volumetric control added in a form of cylinder shown in Figure 3.5.

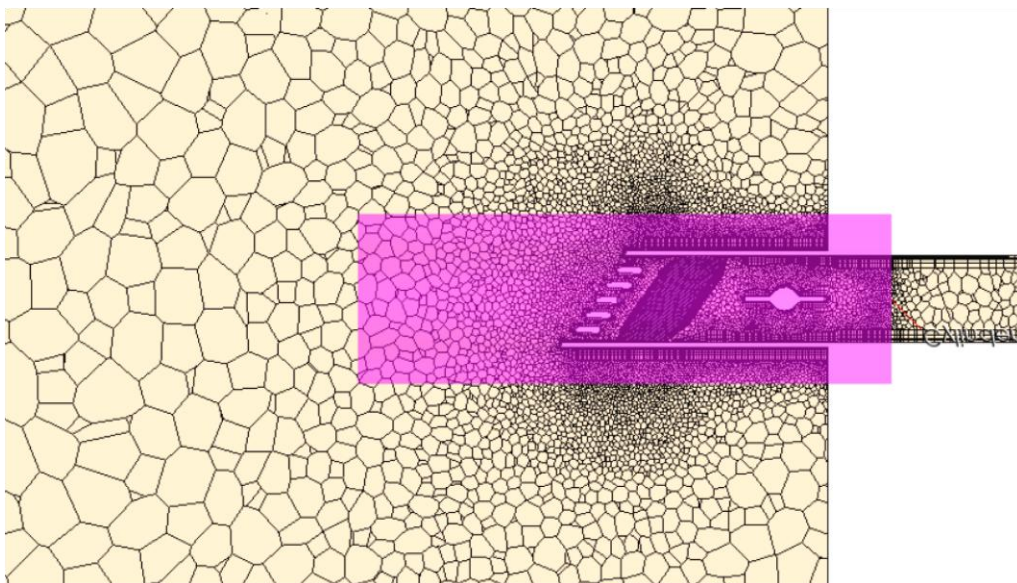


Figure 3.5 Cylindrical volumetric control

Overall cell number: 1 200 000 (approximated).

Physics

- Gas with constant density
- Steady flow
- Turbulence
 - o K- ϵ
 - o RANS
 - o Two-layer All y+ Wall treatment
- Segregated flow solver

- Flow rate at inlet is $80,6 \text{ m}^3/h$.

3.4 Processing

The simulation was stopped by user after approximately 700 iterative steps with residuals shown in Figure 3.6.

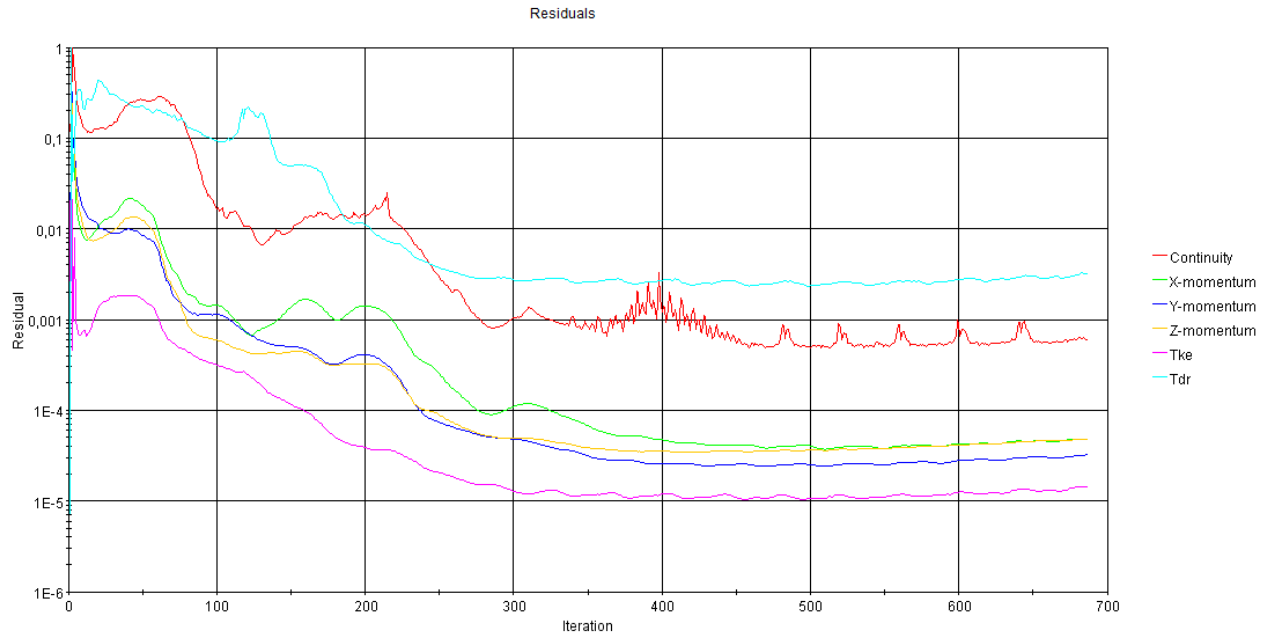


Figure 3.6 - Residuals in STAR-CCM+ CFD simulation

3.5 Post-processing

Post processing workflow went as follows:

- 1) Creation of Presentation grid in STAR-CCM+ (that has the same properties as horizontal and vertical traverse grids in the experiment described before) and grid data update
- 2) Export data in csv format to MS Excel
- 3) Adapting the format of data to importable format to developed MATLAB function for flow border identification
- 4) Import of data to MATLAB, flow border identification and angles computation.

The velocity field in horizontal plane can be seen in Figure 3.7

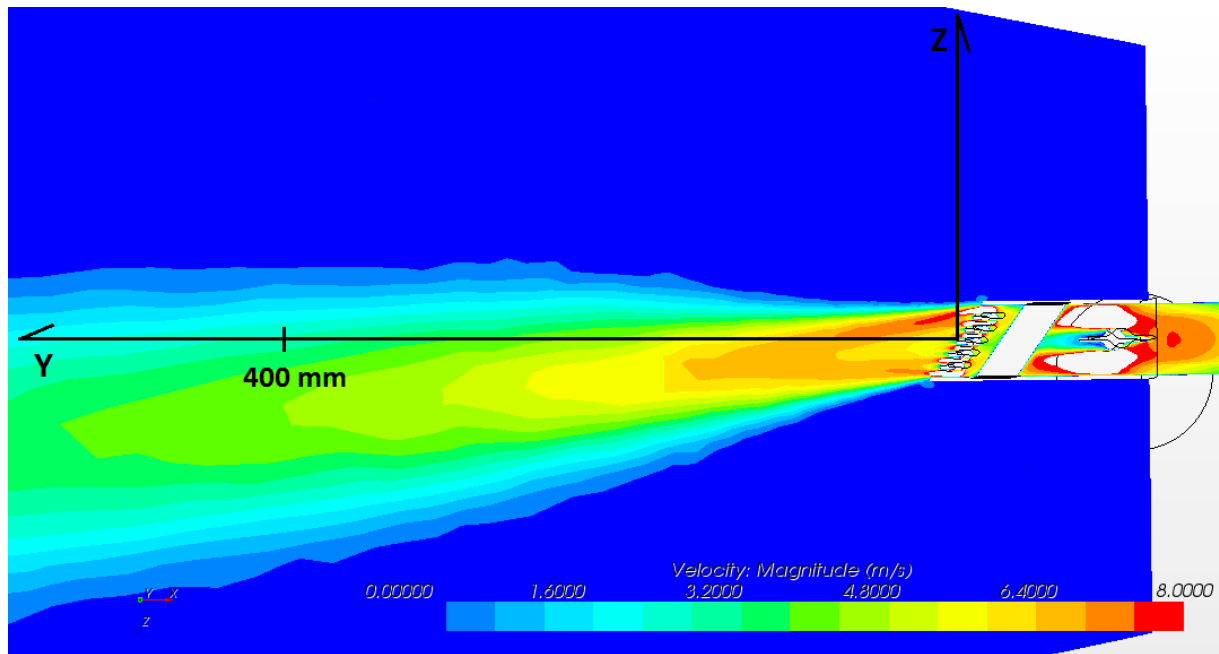


Figure 3.7 Velocity in horizontal plane - CFD result

Angles comparison

Horizontal angles

Flow rate	Case/Angle	$+\beta$ [°]	$-\beta$ [°]	φ [°]	γ [°]	K_s [-]
$80,6 \text{ m}^3/\text{h}$	CFD	3,18	-14,99	-5,90	18,17	4,31
	HWA	10,04	-13,86	-1,91	23,9	3,19

Table 3.2 Horizontal angles

Vertical angles

Flow rate	Case/Angle	$+\alpha$ [°]	$-\alpha$ [°]	ω [°]	δ [°]	K_s [-]
$80,6 \text{ m}^3/\text{h}$	CFD	5,90	-2,27	1,82	8,17	9,84
	HWA	6,14	-4,9	0,62	11,04	7,24

Table 3.3 Vertical angles

Table 3.2 and Table 3.3 show the comparison between simulation and experimental data. The can be due to uncertainty of simulating model (e.g. physics setting or geometry simplifications) and probably also due to border search algorithm. Probably leading problem is the physics setting of flow to „steady“, even though the flow is unsteady (based on experimental data). Interesting step here would be conducting unsteady simulation with more time steps and then comparing the reset with steady simulation.

On the other hand, the simulation was prepared and conducted in a fiction of measurement time and it gives us a first guess how the experiment should be e.g. positioned, how the measuring planes should be oriented etc.

Conclusion

This thesis contains a research done on different possibilities in air velocity measurement with a hot wire anemometry experiment on the test track of The Department of Thermodynamics and Environmental Engineering.

The experiment was a part of a broader range of activities so the conditions and goals were adapted for highest gain possible. The measurement track was put back into operation in 2013 after few years being unused and then later in 2014/2015 new components (A/D board, new automatic calibrator, air filter) were fit in by the author.

The measurement of air velocity profiles was conducted to support CFD models done by Ing. Niedoba for two air flow rates ($33,5 \text{ m}^3/\text{h}$ and $80,6 \text{ m}^3/\text{h}$) and 4 experimental setups were identified to be examined.

For the use of visualization, a new MATLAB-based program for easier and user more friendly operation was developed, and it is able to carry out a quality assessment of a specified plane automatically. Quality measures are further expanded from previous theses and the vent is evaluated based on them.

The calculation of uncertainty of flow rate measurement, setting and HWA method is then carried out to quantify the repeatability of the measurement done on the test track and after evaluating the described cases, there are new findings presented and new questions to be asked.

Some of the important findings are following - the presence of a bend in an air conduit has effect on flow angular deviations from both horizontal and vertical axes. Also, the presence of an air flow rectifier in a bend has a positive impact on turbulence distribution in perpendicular planes which is beneficial for front window defrosting (in winter) but it is also lowering the effect of cooling or heating of passengers on front seats.

The same test track is used for both smoke method visualizations and HWA and the air flow is not filtered, which is lowering the lifespan of probes. Also, there was only one wire probe used which is not direction-sensitive. The jet border is then assessed only by the velocity information and it can be distorted by a shear layer flow which is not necessarily in the same direction as the primary flow. Knowing this, it would be advised to conduct a measurement with two or ideally three wire probe at the specific points to prove or disprove this assumption.

Bibliography

1. Classic car catalogue. In., 2015, vol. 2015. Cit[15.4.2015]. Available from <<http://www.classiccarcatalogue.com/NASH%201954.html>>
2. Airflow_Lufttechnik_GmbH. Inteligentní tlakový převodník PTSXR. Cit [15.4.2015]. Available from < <http://www.airflow.cz/pdf/datasheets/ptsxrk.pdf>>., 2015.
3. Awbi, H. *Ventilation of Buildings*. In.: Taylor & Francis, 2003, p. 522.
4. Brunn, H., H. *Hot-Wire Anemometry: Principles and Signal Analysis*. In. Oxford: Oxford University Press, 1995, p. 536.
5. Caletka, P. *Hodnocení funkčnosti větrací vyústky pro kabinu osobního vozu*. Brno University of Technology, 2014.
6. Comte-Bellot, G. *Hot-Wire Anemometry*. *Annual Review of Fluid Mechanics*, 1976, 8(1), Cit [15.4.2015]. Available from < <http://www.annualreviews.org/doi/abs/10.1146/annurev.fl.08.010176.001233>>. P.209-231.
7. Daily, S. *Automotive Air Conditioning and Climate Control Systems*. In., 2006, p. 432.
8. Dantec. *Measurement principles of CTA*. In., Cit [25.5.2015], Available from < <http://www.dantecdynamics.com/measurement-principles-of-cta>>. 2013.
9. Dantec AND Dynamic. *Measurement principles of LDA*. In.: Dantec Dynamics, Cit [23.5.2015]. Available from < <http://www.dantecdynamics.com/measurement-principles-of-lda>>. 2015.
10. Dantec_Dynamics. *Single-sensor gold-plated wire probes*. Cit [24.5.2015]. Available from < <https://www.dantecdynamics.com/single-sensor-gold-plated-wire-probes>>. In., 2013.
11. Gebauer, G. *Vzduchotechnika*. In H. Horká. 2005, vol. 1.
12. Honus, S. *Matematické modelování fyzikálních a chemických jevů s využitím metod CFD a DEM*. In. Ostrava, 2014.
13. Janotkova, E. *Technika prostředí*. In. Brno, 2014, vol. 1, p. 58.
14. Jørgensen, F., E. *How to measure turbulence with hot-wire anemometers (practical guide)*. In., 2002.
15. Konečný, J. *The laboratory thermometer with sensor Pt100*. Brno University of Technology, 2011.
16. Ležovič, T. *Experimentální analýza proudu vzduchu z ofukovače osobního automobilu s využitím žárového anemometru a návrh hodnocení kvality ofukovače*. 2011a.
17. Ležovič, T., F. Lízal, J. Jedelský and M. Jícha *HVAC automotive vents evaluation and their performance*. HVAC&R Research, 2013/11/17, 19(8), 1073-1082.
18. Lízal, F. *Větrání kabiny vozidla - rychlostní pole v oklí výustek přístrojové desky*, Brno University of Technology, 2007.
19. Nový, R. *Technika prostředí*. Edition ed. Praha: Nakladatelství ČVUT, 2006.
20. Palenčár, R., F. Vdoleček and M. Halaj *Nejistoty měření I: Vyjadřování nejistot*. Automa, 2001, 7(7-8), 50-54.
21. Pavelek, M. *Interaktivní Grafický software pro termodynamické výpočty směsí plynů a par - Vlhky vzduch 3.0*. In P. Snášel. 2010.
22. Pavelek, M. *Přednášky Experimentální metody II*. In. Brno, 2015.
23. Volavý, J. *Přednášky ITM*. In., 2015.
24. ČNI. *ISO 5167 - Určování průtoku tekutin pomocí snímačů diferenčního tlaku vložených do zcela zaplněného potrubí kruhového průřezu*. In. Praha: Český normalizační institut, 2003.

Note: EndnoteWeb MicrosoftWord plug-in was used for citations management according to ISO 690.

List of symbols

a	Orifice vertical dimension,	$[m]$
	Calibration constant	$[-]$
	Acceleration	$[m/s^2]$
	Velocity of sound	$[m/s]$
A	Calibration constant	$[-]$
	Cross section area	$[m^2]$
b	Orifice horizontal dimension	$[m]$
	Calibration constant	$[-]$
B	Calibration constant	$[-]$
c	Specific heat of the fluid	$\left[\frac{J}{kg \cdot K}\right]$
C	Flow rate coefficient	$[-]$
d	Diameter	$[m]$
dx	Elementary wire length	$[m]$
D	Air flow diameter	$[m]$
e	Error voltage	$[V]$
E	Output voltage from anemometer	$[V]$
	Voltage range of A/D board	$[V]$
F	Force vector	$[N]$
g	Gravitational constant	$[m/s^2]$
Gr	Grashof number	$[-]$
h	Convective heat-transfer coefficient	$\left[\frac{W}{m^2 \cdot K}\right]$
I	Electrical current	$[A]$
k	Coefficient of velocity field	$[-]$
	Calibration constant	$[-]$
	Thermal conductivity	$\left[\frac{W}{m \cdot K}\right]$
K	Constant of air vent	$[-]$
m	Weight	$[kg]$
M	Mach number	$[-]$
n	Number of measurements	$[-]$
	Number of bits of A/D board	$[-]$
Nu	Nusselt number	$[-]$
p	Pressure	$[Pa]$
P	Perimeter	$[m]$
Pr	Prandtl number	$[-]$
q	Flow rate	$[kg/s]$
Q	Flow rate	$[m^3/h]$
\dot{Q}	Heat flux	$[W]$
R	Resistance	$[\Omega]$
Re	Reynolds number	$[-]$
S	area	$[m^2]$
T	Temperature	$[^{\circ}C]$
Tu	Turbulence intensity	$[\%]$
u	Uncertainty	
U	Flow velocity	$[m/s]$
v	Velocity	$[m/s]$

w	Velocity	[m/s]
\bar{w}	Average velocity	[m/s]
x	Length	[m]
ΔU_{cal}	Calibrator uncertainty	
ΔU_{fit}	Linearisation uncertainty	

Greek symbols

α	Contraction coefficient	[–]
	Vertical angle	[°]
β	Correction coefficient on momentum	[–]
	Volume coefficient of expansion	[–]
	Horizontal angle	[°]
β_0	Momentum correction factor for non-uniform Velocity distribution	[–]
η	Efficiency	[–]
ε	Emissivity	[–]
	Expansion coefficient	[–]
δ	Angle of spread - vertical	[°]
μ	dynamic viscosity of the fluid	$\left[\frac{kg}{m \cdot s} \right]$
κ	Ratio between free cross-section (cross-section area of gaps in the vent) and nominal cross-section area S_n	[–]
	Isentropic exponent of gas	[–]
σ	Stefan-Boltzmann constant	$\left[\frac{W}{m^2 K^4} \right]$
ω	Axis angle - vertical	[°]
ρ	Density of fluid	$\left[\frac{kg}{m^3} \right]$
v	Spread angle of air jet	[°]
γ	Angle of spread - horizontal	[°]
φ	Relative humidity	[%]
	Axis angle - horizontal	[°]
θ	Probe positioning uncertainty	[°]
χ	Electrical resistivity	[Ω. m]

List of indexes

a	Ambient
b	Breathing
	Barometric
c	Non-axial
$c, cond$	Conduction

<i>conv</i>	Convection
<i>d</i>	Dynamic
<i>e</i>	Evaporation
	Electrical
<i>f</i>	Flow
<i>fc</i>	Forced convection
<i>h</i>	Hole
<i>m</i>	Metabolic
	Mass
<i>n</i>	Nominal
	Rev velocity
<i>p</i>	Prong
<i>r</i>	Radiation
	Rectangular
<i>s</i>	Static
	Storage
	Surroundings
<i>t</i>	Total
<i>V</i>	Volume
<i>w</i>	Wire
<i>x</i>	axial
<i>y</i>	transverse
0	initial
1.. <i>n</i>	index

List of annexes

1. File “Inventor” – contains Autodesk Inventor models of vent, piping, flap, flow rectifier
2. File “Profily” – contains m. file with program and measured data
3. File “Tecplot” – contains .lay files and data files for visualization
4. File “Uhly” – contains m. file and data files for angles determination
5. File “konstanta_vyustky.m” – m. file used for determination of vent constant